sustainability

MDPI

Article

A Comparative Environmental Life Cycle Assessment of Dynamically Wound FRP Reinforcing Bars for Additively Manufactured Concrete Structures

Sophie Viktoria Albrecht [1,*,†], Philip Thiele [2,*,†], Dennis Dittmar [2], Tom Rothe [2], Christian Hühne [2] and Charlotte Thiel [1]

[1] Department of Construction Materials, OTH Regensburg, Galgenbergstraße 30, 93053 Regensburg, Germany; charlotte.thiel@oth-regensburg.de
[2] Institute of Mechanics and Adaptronics, TU Braunschweig, Langer Kamp 6, 38106 Braunschweig, Germany; christian.huehne@dlr.de (C.H.)
* Correspondence: sophie.albrecht@oth-regensburg.de (S.V.A); philip.thiele@tu-braunschweig.de (P.T.)
† These authors contributed equally to this work.

Abstract

Integrating non-corrosive reinforcement offers a transformative opportunity to reduce concrete cover and enable material-efficient additive manufacturing. However, compatible reinforcement strategies remain rare, and their environmental performance is largely unquantified. This study evaluates the environmental impact of basalt- and glass fibre-reinforced polymers produced using a Dynamic Winding Machine for on-site, free-form production in digital construction. Tensile tests yielded short-term tensile strengths of 804 MPa (glass) and 1106 MPa (basalt), which were used in structural beam calculations across ten additive manufacturing concrete mixtures. To ensure comparability, the reinforcement materials and concrete mixtures were assessed on an equal mass and volume basis, while the beam case study was evaluated based on equivalent structural performance. These data informed a cradle-to-gate (A1–A3) Environmental Life Cycle Assessment benchmarking in-house-produced reinforcements against steel and carbon fibre-reinforced polymers. Averaged across the mixtures, the range of Global Warming Potential total indicates that glass and basalt fibre-reinforced polymers achieve 13% and 15% lower greenhouse gas emissions compared to conventional steel, whereas carbon fibre-reinforced polymers exhibit the highest Global Warming Potential total. Ultimately, the results substantiate free-form fibre-reinforced systems, particularly when combined with additive manufacturing and alternative concrete formulations, as a key strategy for advancing sustainable and climate-resilient construction.

Keywords: environmental impact; Environmental Life Cycle Assessment (E-LCA); Additive Manufacturing in Construction (AMC); Basalt Fibre Reinforced Polymers (BFRP); Glass Fibre Reinforced Polymers (GFRP); Dynamic Fibre Winding (DFW)

Check for updates

Academic Editors: Rajab M. Abousnina and Magdi Almabrok

Received: 22 September 2026
Revised: 23 October 2026
Accepted: 28 October 2026
Published: 3 November 2026

Copyright: © 2026 by the authors. Licensee MDPI, Basel, Switzerland. This article is an open access article distributed under the terms and conditions of the Creative Commons Attribution (CC BY) license.

1. Introduction

Concrete is the most widely used construction material worldwide and simultaneously one of the largest contributors to global CO_2-eq emissions, with the cement industry responsible for around 6% of anthropogenic greenhouse gases [1]. As urbanisation and infrastructure demands continue to rise, reducing the environmental impact of concrete structures has become a critical challenge in addressing climate change [2]. At the same

time, the industry faces a shortage of skilled workers [3]. Therefore, new, innovative strategies are needed to reduce environmental impact, which align with higher automation that requires fewer workers.

Additive Manufacturing in Construction (AMC) offers great potential for resource-efficient, automated manufacturing processes [4]. By enabling precise, layer-wise material deposition, Additive Manufacturing (AM) reduces material waste and the need for conventional formwork while promoting a high level of geometrical form freedom [5]. This enables the fabrication of individualised, functionally optimised concrete elements.

Traditionally, steel reinforcement is manually wired and embedded in concrete components to compensate for concrete's lack of tensile strength. Due to steel's corrosion susceptibility and the need to satisfy fire protection requirements, a minimum concrete cover is required to ensure both durability and structural safety under environmental and thermal exposure conditions [6]. This additional concrete not only increases material consumption and structural self-weight but also significantly contributes to the overall environmental impact, particularly due to the high carbon intensity of cement production [7].

These limitations become even more pronounced in the context of additive manufacturing of concrete, where highly automated production processes and geometrically complex, individualised structures challenge the applicability of conventional reinforcement solutions. To fully exploit the design freedom offered by additive manufacturing, reinforcement systems must be compatible with digital fabrication workflows and adaptable to non-standard geometries.

Among the most promising reinforcement alternatives for additively manufactured concrete are fibre-reinforced polymer (FRP) systems. In structural applications, fibres are embedded in a polymer or mineral matrix to form reinforcement bars or strands. The matrix binds and stabilises the fibres, shields them from mechanical and environmental damage, and ensures effective stress transfer from the surrounding concrete to the entire reinforcement cross-section [8]. Common FRP reinforcement systems include basalt (BFRP), glass (GFRP), or carbon fibre-reinforced polymers (CFRP) [9–12]. In combination with additive manufacturing, FRP reinforcement enables the realisation of free-form structural elements and offers the potential for force-flow-oriented reinforcement layouts following principal stress trajectories, thereby improving material utilisation [13].

The potential of this approach has already been demonstrated by Mechtcherine et al. [14], who combined 3D-printed concrete with freely formable mineral-impregnated CFRP reinforcement, achieving a reduction in reinforcement weight of more than 90% compared to a conventional steel-reinforced balcony structure. These findings demonstrate the potential of combining FRP reinforcement and additive manufacturing to reduce material consumption while maintaining structural performance.

The FRP materials examined differ in their properties and advantages, covering a wide range of available FRP reinforcements. BFRP is gaining significant attention due to its balance of mechanical properties, durability, and environmental advantages [11,15]. Derived from naturally occurring basalt rock, its production process is relatively simple and eco-friendly compared to synthetic fibres. While GFRP and CFRP reinforcements also provide superior durability and mechanical benefits, they offer specialised advantages. Glass fibres are widely accessible and relatively cost-effective. In structural applications, alkaline-resistant (AR) or electric corrosion-resistant (E-CR) glass is used because it offers greater resistance to degradation in alkaline concrete pore solutions than conventional glass fibres. At the high end of the performance scale, carbon fibres provide outstanding tensile strength, durability and stiffness [11]. Table 1 gives an overview of the characteristics of commercially available FRP reinforcement systems.

Table 1. Overview of commercially available FRP reinforcement systems.

Name	Tensile Strength in MPa	Young's Modulus in GPa	Density in kg/m^3	Rebar Costs [16] in EUR /kg
GFRP [17]	1000	60	2200	8
BFRP [18]	1350	55	1910	6
CFRP [19]	2300	140	1500	100

The use of non-corrosive fibre reinforcements aligns with the goals of sustainable construction. The concrete cover that serves to protect steel reinforcement can be reduced, which lowers the required concrete volume. The reduction depends on structural, fire, durability, and serviceability requirements. In addition, the absence of reinforcement corrosion can extend the service life of structures with minimal maintenance [11,20]. In the context of global efforts to mitigate climate change, these materials represent a strategic opportunity to lower the embodied carbon in concrete structures without sacrificing structural performance or durability [9,10,20].

In line with these considerations, multiple Environmental Life Cycle Assessment (E-LCA) studies report lower climate change impacts for FRP-reinforced concrete beams compared to steel-reinforced counterparts when equivalent structural performance is ensured. These findings, however, are derived from beam-specific case studies and remain strongly dependent on geometry, loading conditions, and design assumptions [21–23]. Integrating E-LCA into the early stages of design is increasingly recognised as essential for achieving low-carbon construction, particularly as digital fabrication introduces new material systems and design freedoms. Early-stage E-LCA enables designers to evaluate environmental impacts when design decisions still have the greatest influence and can be modified at minimal cost [24]. Recent research emphasises that E-LCA integration during early design supports more sustainable architectural and structural outcomes by enabling environmental criteria to guide material selection, geometric optimisation, and fabrication strategies. This is especially relevant in digital fabrication, where novel processes and materials require systematic assessment to verify whether they deliver environmental benefits over conventional methods [25].

However, fibre reinforcement has several environmental drawbacks, including the high energy demand of fibre production, the use of petrochemical-based polymer matrices, limited recyclability of fibre-reinforced composites, and challenges in separating fibres from concrete at the end of life, which can complicate recycling processes and increase environmental impacts.

This paper assesses the potential of glass and basalt fibre reinforcement in 3D-printing concrete mixtures, emphasizing their role in advancing more sustainable, climate-resilient construction practices. The study investigates whether in-house manufactured GFRP and BFRP reinforcement, produced using a Dynamic Winding Machine (DWM) from various endless fibre materials and a room-temperature-curing epoxy matrix, can serve as a sustainable alternative to conventional steel and CFRP reinforcement in concrete construction. This production technology enables free-form geometries and on-site production aligning with automation and material efficiency requirements. Through tensile testing, the mechanical properties of these custom reinforcement bars (rebars) were evaluated and subsequently used to calculate a simple, reinforced beam element. This forms the basis for an environmental impact comparison against conventional steel and high-performance CFRP reinforcement across multiple sustainability scenarios from cradle to gate (A1–A3). These scenarios include a multi-stage comparison, which provides detailed analyses of the materials and the resulting environmental impact per mass and mechanical properties, as

well as in the component composite. Various concrete mixtures used for AM are considered. Therewith, for the first time, the environmental impact of the DWM is evaluated, taking into account both the production process and the reinforcement strands to demonstrate the sustainability potential of customisable reinforcement methods, as the custom-developed DWM manufacturing system has not previously been assessed through an environmental life cycle assessment.

The results serve as decision support in selecting the most sustainable material composition. Moreover, they provide a foundation for future research on environmentally and design-optimised construction components.

2. Methodology for FRP Reinforcement Characterisation

In this study, four reinforcement materials are analysed regarding their environmental impact when combined with concrete mixtures in the field of AM. To evaluate their viability as sustainable reinforcements, in-house-manufactured E-CR GFRP and BFRP rebars were tested and simulated in AM concrete mixtures and one conventional control mixture. Their mechanical performance and environmental impacts are benchmarked against conventional ribbed steel and CFRP rebars, representing the current standard and a high-performance alternative, respectively. When possible, standards are used for test design and calculations. In addition, information from manufacturers is consulted to ensure comparability and analysis of potential. This comparative approach enables a holistic assessment of the trade-offs among different reinforcement systems for concrete construction in terms of structural efficiency, durability, and sustainability.

2.1. Dynamic Fibre Winding

A DWM was developed to enable the production of free-form reinforcement patterns, optimising the use of fibre reinforcements [26]. The reinforcement strands consist of primary endless fibres for the absorption of tensile forces, a secondary yarn for surface profiling to enhance concrete bonding, and a room-temperature-curing epoxy resin. The strands enable robotic winding into the desired shape, where they are held in place by support structures until full curing has been achieved. The compact build volume of the modular process enables on-site fabrication, reducing transport-related impacts.

The DWM consists of four main sections (see Figure 1): The primary fibres are guided from a storage system through a resin bath, where they are impregnated (1). After the removal of excess resin, the strand runs through a rotating hollow shaft, which adds a secondary yarn to the primary fibres, structuring the reinforcement surface for better bonding properties. A hysteresis brake enables variation in the undulation by varying the moment of resistance of the secondary yarn, resulting in an adjustable surface geometry (2). An active pull-out unit ensures consistent production quality by synchronising the extrusion speed of the primary fibres with the winding thread of the secondary yarn (3). Before the reinforcement strand is connected by an outlet to the end-effector of a robot for automated integration, a tension and storage unit ensures the pre-tension of the strand inside the machine and compensates for movements and accelerations of the robot (4) [26].

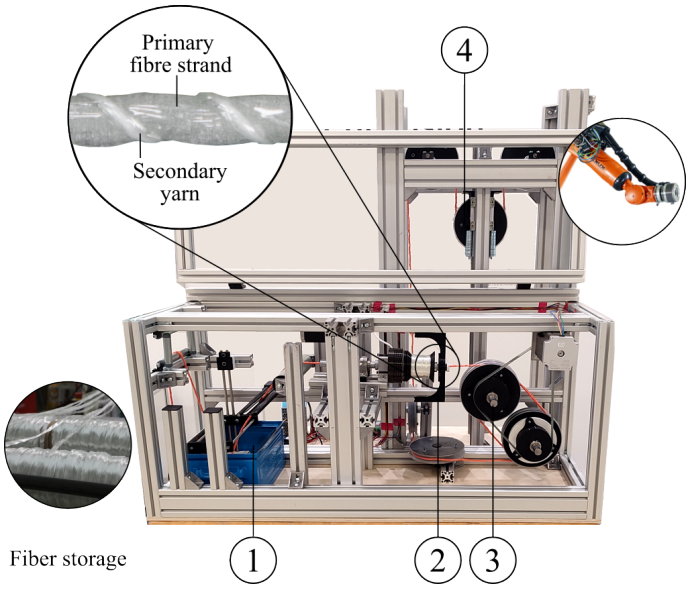


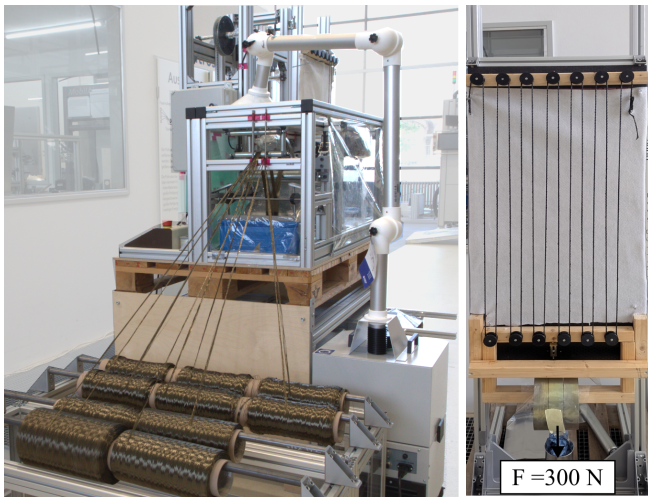
Figure 1. Dynamic Winding Machine divided in four modules: (1) resin bath and excess resin removal, (2) helix winding unit, (3) pull-out unit, (4) tension and storage unit.

2.2. Rebar Fabrication by Dynamic Fibre Winding

The GFRP and BFRP rebars were produced using the DWM. For this study, a total of 12 specimens of GFRP and BFRP were produced, each from a single production batch. Subsequently, the short-term characteristics of eight randomly selected samples are experimentally validated by standardised mechanical tensile testing. All characterisation and testing results can be found in the corresponding data publication [27]. Nominal diameters with approximately 8 mm are producible without compromising quality [28]. The specimens were designed with a nominal diameter of 4 mm, selected to ensure optimal informational value within studies employing the DWM [28–30]. For E-CR GFRP samples, this results in a total number for primary fibres and secondary yarn of 19608 tex, consisting of two rovings of 9600 tex and a braided secondary yarn from Culimeta EC-9 136 X3 S135 of 408 tex. For the primary strand, PulStrand 4100 from Owens Corning was used. The total number of basalt is 20100 tex, consisting of ten rovings of 2000 tex and a secondary yarn of 100 tex. Basalt fibres BF-17/2000-GTS1-G-A of Deutsche Basalt Faser were used. The matrix material consisted of the epoxy resin system EPIKOTE Resin MGS RIMR 426 combined with EPIKURE Curing Agent MGS RIMH 435, mixed at a weight ratio of 100:26. This resin system offers an average processing window of approximately 120 min at 20 °C.

A notable challenge during rebar fabrication was the preparatory rewinding of the basalt fibre rovings. To achieve a reinforcement diameter of 4 mm, ten rovings of 2000 tex each are required. Consequently, the fibres were manually rewound from the two original spools supplied by the manufacturer onto additional winding cores.

The hysteresis brake was set to a constant value of 100 mA and the thread pitch of the secondary yarn was set to 10 mm for both fibre materials. Figure 2a shows the loading of the machine with the required ten basalt rovings during the production process. The reinforcement strand was manually pulled out of the DWM and fixed in position using a prepared pin board, with the rebars aligned vertically (see Figure 2b). The rebars were subjected to an initial prestress of 2 MPa during curing with additional mass mounted on a connecting rod across the lower winding pins. After production, all rebars were subsequently cured for a minimum of 48 h before being prepared for tensile testing.



(**a**) (**b**)

Figure 2. Rebar production using the DWM (**a**) loading of the DWM with basalt fibre rovings, (**b**) board for curing of the basalt rebars with an applied load of 2 MPa.

2.3. Geometric Properties

After complete curing, the actual diameters of the rebars and their fibre volume content were evaluated [27]. To calculate the average diameter, measurements were taken at 100 mm intervals along the bar. At each interval, three readings were recorded at 60° increments around the cross-section to account for ovality and surface imperfections. Based on the mass of the fibres and the total volume of the bar, the fibre volume content φ was determined for each specimen (fibre volume V_f, total rebar volume V_{rebar}):

$$\varphi = \frac{V_f}{V_{rebar}} \quad (1)$$

2.4. Short-Term Property Testing Method of Produced Reinforcements

Tensile tests were performed in accordance with the ASTM D7205/D7205M-21 [31] standard for continuous fibre-reinforced polymer matrix composite rebars. The tests enable the evaluation of the short-term tensile strength and Young's modulus. Therefore, specimens were cut to a nominal length of 780 mm. To ensure purely axial tensile loading and prevent lateral forces, both specimen ends were embedded in 200 mm-high steel sleeves using the matrix epoxy resin system. To prevent sudden, local force application, all edges of the steel sleeves were deburred, and the sleeves were cleaned before use. At the bottom of the steel sleeves, a plastic cap is used to seal the sleeves and center the rods. The dimensions of the tensile specimens can be seen in Figure 3. A specialised alignment fixture was utilised during embedding to maintain consistent axial alignment. Further description can be found in Rothe et al. [28].

The tensile tests were conducted on an Instron machine type 5584 with an extraction speed of 4 mm min^{-1} under displacement control. The specimens were clamped in the testing rig at a pressure of 100 bar. An extensometer was used, measuring the strain over a gauge length of 60 mm continuously. In addition, the distance traveled by the crosshead of the tensile testing machine between the anchor points (380 mm apart) and the tensile force are recorded. For both reinforcement types (GFRP, BFRP), eight specimens were tested at room temperature seven days after curing, storing and embedding into steel sleeves [27]. This experimental procedure enabled a direct comparison of the mechanical behaviour and failure characteristics between the two material systems under identical testing conditions.

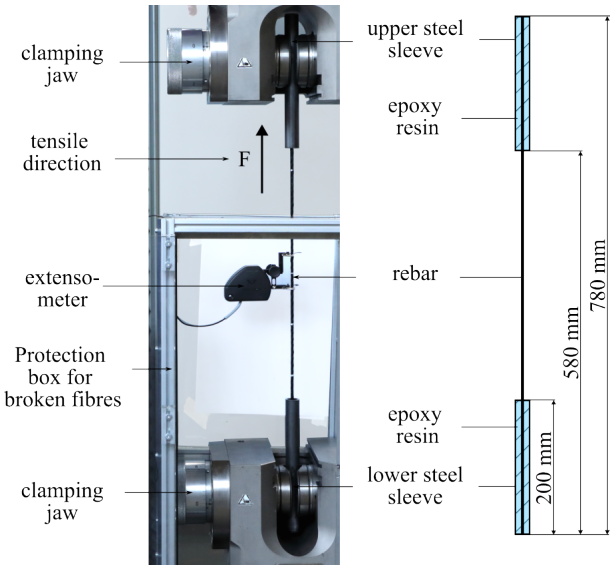


Figure 3. Specimens in the tensile testing machine, with an extraction speed of 4 mm min^{-1}, and tensile specimen dimensions.

3. Environmental Life Cycle Assessment

An E-LCA is conducted to quantify the environmental impacts associated with the selected reinforcement materials and concrete mixtures.

3.1. Goal and Scope

For the E-LCA, the framework established in ISO 14040 and ISO 14044 was applied [32, 33]. The Software openLCA 2.5 and the database ecoinvent 3.11 cut-off, as well as several Environmental Product Declarations (EPDs), adhering to ISO 14025 and EN 15804, were used [6,34]. The life cycle phases A1–A3, cradle-to-gate, are analysed in this study, covering raw material production, transport, manufacturing, electricity consumption, and DWM-related impacts, including both wear parts and durable components. Production losses, transportation losses, and waste streams are excluded from the assessment.

The geographical scope is Europe, where such regional data are unavailable; data for specific European countries are chosen; and finally, global datasets. Four complementary environmental evaluations are conducted to assess the sustainability of reinforcement materials, concrete mixtures, and the Dynamic Fibre Winding Machine and their application at the structural level.

Initially, four reinforcement materials are analysed using the functional unit of 1 kg and subsequently normalised with respect to their mechanical performance characteristics. This approach enables a consistent comparison between conventional steel reinforcement and three FRP alternatives (see Table 1).

In parallel, ten additively manufactured concrete mixtures of eight different compressive strength classes are evaluated using the functional unit of 1 m^3. Additionally, an assessment of conventional concrete mixtures with equivalent strength classes is conducted. This allows for a direct comparison between additively manufactured and conventional concrete systems under consistent, comparable environmental assumptions.

In the following step, the DWM used for fibre reinforcement production is evaluated independently. Its environmental impacts are normalised both per printing hour and per 1 m of produced fibre reinforcement, considering a service life range of 5000 to 15,000 operating hours, thereby capturing the influence of machine utilisation on overall impacts.

The results of the previously described environmental assessments are subsequently integrated into a structural-level case study.

Based on the range of environmental impacts observed for the different reinforcement materials and concrete mixtures, a minimum- and maximum-value approach is applied, using the lowest and highest Global Warming Potential total (GWP-t) values at beam level, thereby capturing the variability and uncertainty of environmental impacts within the European context. To support this approach, EPDs were systematically collected and evaluated from the following sources: international EPD [35], epd-global [36], the Kiwa-Ecobility database [37], and the IBU database [38].

To establish a consistent basis for the E-LCA, a steel-reinforced concrete beam with a span of 4 m and a cross-section of 0.2 m × 0.4 m is used as the reference component for comparing steel and FRP reinforcement systems under identical loading conditions (see Figure 4). The reference utilises a standard C30/37 concrete mixture with a characteristic compressive strength f_{ck} of 30 MPa and a Young's modulus E_c of 33 GPa and is reinforced with 8 mm diameter steel B500B rebars. It carries a permanent load g_k = 10 kN/m and a variable load q_k = 8 kN/m. Only bending and shear are considered, as the assessment focuses on mechanical properties and does not cover torsion, fire resistance or manufacturability.

The comparison covers four reinforcement materials (B500B, GFRP, BFRP, CFRP) and ten concrete mixtures. For each mixture, the cross-section is derived from the reference beam so that all variants are structurally comparable, which is described in detail below. The FRP variants are 5 mm lower in height owing to the reduced cover (cf. Section 5.4). The required reinforcement of each variant was determined in SOFiSTiK. The required reinforcement areas are converted into masses, which, together with the net concrete volume, form the input of the E-LCA. A reinforcement diameter of 8 mm was adopted for all reinforcement materials as a representative compromise: it corresponds to the smallest bar diameter that can be specified in SOFiSTiK and to a diameter that can be produced with the DWM. Although the characteristic values were determined using 4 mm rebars, earlier studies have shown that they can be applied to 8 mm rebars [28]. The design assumptions, reinforcement layouts and all calculation inputs and results are provided in the accompanying dataset [27].

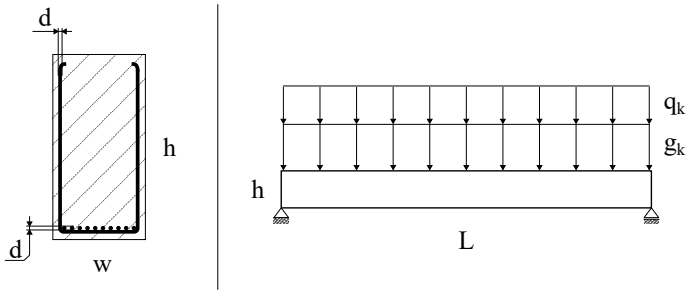


Figure 4. Investigated beam for material variation (length L = 4 m, reinforcement diameter d = 8 mm, permanent load g_k = 10 kN/m, variable load q_k = 8 kN/m, width w and height h).

The structural behaviour and design of the reinforcement of the concrete beam were evaluated using SOFiSTiK FEA 2026 (Version 1.0.361). The beam was discretised using a 1D cross-section-based beam element. The mechanical properties of the four reinforcement types, specifically their distinct stress–strain relationships, were integrated into the simulation environment to analyse the structural response under the defined loading conditions. The specific mechanical characteristics of the self-produced reinforcements, derived from the experimental tensile tests with the assumed long-term behaviour (as discussed in Section 4.3) were taken into account. The assumptions are mainly used for longitudinal reinforcements. Due to the worse performance of FRP reinforcements as cross reinforcement compared to steel, an additional reduction factor (including the long-term reduction) is applied to the mechanical performance of FRP stirrups based on the manu-

facturer's data sheet for straight rebars and stirrups (Schöck Combar [17]). This results in a reduction of tensile strength to approximately a quarter of the short-term mean value, resulting in approximately 191 MPa (GFRP) and 263 MPa (BFRP). No characterisation tests were performed on the DWM stirrups, so the factor is a transferred assumption. The required stirrup reinforcement was determined automatically in SOFiSTiK using the reduced strength. No bend radius was specified, so the effect of the bend is represented only by the reduction factor. The corner strength of continuously wound fibres may differ from that of factory-bent rebars, since it depends on the bend radius, the fibre type and the production method. The behaviour of DWM reinforcement at bent sections is therefore an interesting subject for further research, e.g., through tensile tests on bent specimens with varying bend radii. The influence of this assumption is discussed in Section 6.1. To account for the different concrete mixtures, the already embedded materials in SOFiSTiK were used and slightly adjusted to the specific properties. By defining the custom material curves of the reinforcements and the concrete mixtures, the simulation accurately reflects the reduced stiffness and increased fracture strain of the GFRP and BFRP systems compared to industrial benchmarks embedded in concrete for AM processes. To ensure consistency within the calculation, a uniform diameter of 8 mm was assigned to all reinforcement materials and types. To evaluate the minimum of needed reinforcement, the default value for the minimum needed was set to 0.01 cm^2 per unit.

The cross-sectional geometry of the beam was designed independently of SOFiSTiK and was subsequently provided as an input parameter for the reinforcement calculation. A function of the concrete's compressive strength and Young's modulus was proportioned, with the aim of balancing flexural load-bearing capacity and stiffness relative to the reference configuration, rather than minimising material use alone. All calculations were implemented in Python 3.12.11. The full code can be viewed in the accompanying data publication [27].

The cross-section was constrained to a fixed aspect ratio, where the height is twice the width ($h = 2b$). The following proxy quantities are used as approximate values to describe the unreinforced concrete cross-section. The flexural capacity proxy (Ultimate Limit State, $\mathrm{ULS}_{\mathrm{proxy}}$) considers the characteristic compressive strength f_{ck}, while the stiffness proxy (Serviceability Limit State, $\mathrm{SLS}_{\mathrm{proxy}}$) takes the characteristic Young's Modulus into account:

$$ULS_{\mathrm{proxy}} = f_{ck}\, b\, h^2\,, \qquad SLS_{\mathrm{proxy}} = E_c\, b\, h^3 \tag{2}$$

The constant factor is omitted, as the aim is to calculate normalised ratios. It should be noted that the proxy quantities serve as simplified scaling indicators of flexural capacity and stiffness to obtain a consistent initial cross-section geometry prior to the reinforcement design. Normalising these proxy quantities to the reference cross-section of C30/37 (0.2 m × 0.4 m) yields the dimensionless equivalence ratios:

$$\mathrm{ULS}_{\mathrm{ratio}} = \frac{ULS_{\mathrm{proxy}}}{ULS_{\mathrm{proxy,ref}}}\,, \qquad \mathrm{SLS}_{\mathrm{ratio}} = \frac{SLS_{\mathrm{proxy}}}{SLS_{\mathrm{proxy,ref}}} \tag{3}$$

For each concrete class, the width b was determined by minimising the following weighted objective function:

$$f(b) = A(b) + w\,(\mathrm{ULS}_{\mathrm{ratio}}(b) - 1)^2 + w\,(\mathrm{SLS}_{\mathrm{ratio}}(b) - 1)^2 \qquad \text{with} \qquad A(b) = 2b^2 \tag{4}$$

$A(b) = 2b^2$ denotes the cross-sectional area, and the two remaining terms penalise the squared deviation of the load-bearing (ULS_{ratio}) and stiffness (SLS_{ratio}) equivalence ratios from unity, weighted by the factor w. The width b was obtained by minimising Equation (4) using a bounded scalar minimisation routine (scipy.optimize.minimize_scalar, method "bounded" from the SciPy library) with weighted factor $w = 10$, which lies within the saturated regime in which the solution is governed by the equivalence criteria rather than by the choice of w itself. The search interval is limited by $b \in [0.1\,\text{m}, 0.5\,\text{m}]$.

This formulation should be understood as a compromise solution to analyse the potential rather than an exact fulfilment of both equivalence criteria. For b as a single free geometric parameter under a fixed aspect ratio, ULS and SLS equivalence cannot generally be satisfied simultaneously, since compressive strength and Young's modulus do not scale proportionally across concrete classes. The optimisation, therefore, balances a reduction in cross-sectional area against the combined deviation from both target values, rather than enforcing strict equivalence with either criterion individually.

Overall, the study integrates assessments at the material, process, and structural levels, enabling a comprehensive evaluation of reinforcement systems, concrete mixtures, and the DWM within a consistent cradle-to-gate E-LCA framework.

3.2. Life Cycle Inventory

The life cycle inventory and the EPD collection used in this study are documented and available in [39]. The regional scope for the E-LCA is considered progressively, starting with Europe, followed by Europe without a specific country, then a European country, and finally global. The reinforcements and mixtures were separated in the life cycle phases A1 (raw material supply), A2 (transport) and A3 (production).

3.2.1. Reinforcements

Four reinforcement types were considered in this study. R1 represents the conventional steel reinforcement, whereas scenarios R2–R4 portray the fibre reinforcement scenarios (R2 = GFRP; R3 = BFRP; R4 = CFRP).

For R1, the dataset "reinforcing steel production | reinforcing steel | Cutoff, U–Europe without Austria" was selected, as it already covers all cradle-to-gate life-cycle phases (A1-A3). Therefore, no separate datasets were required.

For the transportation of the raw materials of the FRP reinforcements to the production site, an average distance of 500 km is considered for the fibre reinforcement materials. Hohmann [40] reported transport distances of 1000 km for fobre materials within European supply chains. To represent the combined transport of fibres and resin in a simplified manner, an average transport distance of 500 km was assumed for the FRP constituents.

R2 corresponds to glass fibre reinforcement, consisting of two interwoven glass fibres coated with an epoxy resin. Due to data limitations in ecoinvent, only a single process dataset for glass fibre production was available; therefore, the same dataset was applied to both fibre types. R3 represents basalt fibre reinforcement, with production data based on Fort et al. [41] as no basalt fibre dataset is included in the ecoinvent database. R2 and R3 require electricity as part of the production process; the associated electricity demand was measured using the DWM during the manufacturing of the reinforcements. For R4, the third carbon fibre configuration from Backes et al. [9] was adopted. The production of "credit blend raw fibre" was excluded, as no suitable ecoinvent dataset or EPD could be identified. The exclusion affects 4,44 wt.% of the material composition and should be considered when interpreting the E-LCA results. Likewise, the production of the carbon scrim was omitted in the life cycle phase A3, since the reinforcement considered in this study consists of bar reinforcement rather than mesh reinforcement. In scenarios R2–R4,

the DWM was included in the life cycle phase A3, with an assumed operational service life of 10,000 printing hours.

For the Minimum and Maximum assessment of Global Warming Potential total (GWP-t), a targeted review of available EPDs was conducted for the reinforcement materials considered in this study [39]. A total of ten EPDs were identified for steel reinforcement (steel rebar) originating in Europe or individual European countries, providing a representative, regionally relevant data basis. Furthermore, five EPDs were identified for glass fibre reinforcement. In contrast, the availability of EPD data for alternative fibre-based reinforcements was limited, with only one EPD for basalt fibre reinforcement and another for carbon fibre reinforcement.

3.2.2. Concrete Mixtures

The choice of concrete mix design directly influences not only the environmental impacts of a structural element but also its mechanical performance. To capture this interdependence, ten concrete AM mixtures were selected from a range of publications to represent the diversity of existing mix designs across extrusion and shotcrete 3D printing (see Table 2) [9,42–46].

Table 2. Concrete mixtures, material composition, and compressive strength. Abbreviations: SCMs = Supplementary Cementitious Materials, fa = fly ash, s = sand, ss = silica sand, PVAf = Polyvinyl Alcohol fibre, MC = Methylcellulose, p = plasticiser, sa = set accelerator, st = stabilizer, l = limestone, ggbfs = ground granulated blast furnace slag, VMA = Viscosity Modifying Agent, rca = recycled coarse aggregate, cc = calcined clay, d = defoamer, CSA = Calcium Sulfoaluminate cement, r = retarder.

Name	Cementitious Materials in kg/m^3	SCMs in kg/m^3	Aggregates in kg/m^3	Water in kg/m^3	Admixtures in kg/m^3	Additives in kg/m^3	Compressive Strength in N/mm^2	Source
C1	700.00 CEM I	210.00 fa	670.00 s, 348.30 ss	277.60	-	6.50 PVAf, 7.00 MC	C30/37	[9,47]
C2	600.00 CEM I	-	1258.00 ss	270.00	1.80 p, 36.00 sa, 0.60 st	97.00 l	C60/70	[42]
C3	550.00 CEM I	165.00 fa	659.90 s, 538.30 ss	277.80	-	6.50 PVAf, 5.30 MC	C25/30	[9,47]
C4	376.30 CEM I	378.30 ggbfs	1279.30 s	263.40	5.27 p, 0.75 VMA	-	C45/55	[43]
C5	374.20 CEM I	374.20 ggbfs	900.80 s	261.90	5.24 p, 0.75 VMA	-	C40/50	[43]
C6	370.80 CEM I	370.80 ggbfs	909.40 s, 351.50 rca	259.60	3.34 p, 0.74 VMA	-	C35/45	[43]
C7	331.00 CEM I	331.00 cc	1241.25 s	248.25	16.55 p, 2.00 VMA	165.50 l	C30/37	[44]
C8	155.00 CEM I	-	1600.00 rca	285.00	9.30 p, 3.10 d	18.00 sf, 282.00 l	C20/25	[45]
C9	700.00 CEM III/A	210.00 fa	633.00 s, 332.80 ss	277.80	-	6.50 PVAf, 7.00 MC	C30/37	[9,47]
C10	399.70 CEM III/B	171.30 CSA	909.00 ss	285.00	4.00 p, 3.95 r	317.00 l, 2.80 MC	C12/15	[46]

The selected AM mixtures encompass a broad spectrum of compositions, particularly with respect to cement type and content, resulting in a wide variety of compressive strength classes ranging from C12/15 to C60/75. To facilitate comparison, the concretes are organ-

ised according to both the amount and the type of cement used. Mixture C1 contains a high proportion of Portland cement (CEM I), while C10 utilises a comparatively low proportion of CEM III/B, a ground granulated blast furnace slag cement. The dataset includes mixtures characterised by high Portland cement content (C1 and C2), those incorporating recycled aggregates (C6 and C8), calcined clay (C7), and mixtures designed to minimise environmental impact by using CEM III (C10 and C11).

The exact amounts and ecoinvent processes or EPDs used for each scenario can be found in [39]. If no suitable ecoinvent dataset is available for a given material or process, an EPD adhering to ISO 14025 and EN 15804 is used instead [6,34]. When neither an appropriate ecoinvent dataset nor an EPD can be identified, the material or process is not analysed in the E-LCA. This is only applicable for C2, C8 and C10 where the material has neither an ecoinvent dataset nor an appropriate EPD, but the overall material mass in each mixture is lower than 1% of the overall weight.

For the life cycle phase A1, ecoinvent production processes were used for all materials, except for water. Since water is sourced directly from the tap and does not require transport by truck, a market process dataset was selected instead, as it accounts for the water supply network. For cement, datasets representing specific strength classes were not available; therefore, generic cement datasets from ecoinvent were employed. Similarly, quartz sand is not available as a separate dataset in ecoinvent. Consequently, for all mixtures containing quartz sand, the silica sand dataset was used as a proxy. For mixture C2, no suitable ecoinvent datasets were available for the set accelerator or the stabiliser. Furthermore, no appropriate EPD could be identified for the stabiliser. The same limitation applies to mixture C10, which also contains a stabiliser for which no EPD is available. Mixtures C1, C3 and C9 were originally adopted from Backes et al. [9], where they had previously been analysed using the GaBi software and the CML2001 methodology. In the present study, these mixtures were adapted to the most recent ecoinvent 3.11 database, with only minor modifications made to account for differences in data availability. Mixtures C4–C8 are designed without silica and quartz sand and incorporate fine and coarse aggregate [43–45]. Specifically, C4 contains only fine aggregate, C5 includes both fine and coarse aggregates, and C6 combines fine aggregate with recycled coarse aggregate. The recycled coarse aggregate is modelled per 1 kg functional unit using process and material data reported by Stengel and Kustermann [48]. Mixture C7 represents a formulation whose binder comprises cement, calcined clay, and limestone, developed as a more sustainable materials solution [44]. C8 employs the lowest amount of Portland cement combined with recycled aggregate. Scenarios C9 and C10 utilise ground granulated blast furnace slag cement, specifically CEM III/A and CEM III/B, respectively. C10 is a sustainability-enhanced 3D printing mixture using, as the main components, ground granulated blast furnace slag cement, silica sand, CSA cement and limestone.

In this study, the >32 t EURO 6 truck dataset was selected, as this emission class most accurately represents the current composition of the vehicle fleet operating in Europe [49]. An average transport distance of 100 km was assumed for the raw materials. A transport distance of 100 km for recycled coarse aggregate remains below the critical threshold at which its environmental performance becomes less favourable than that of natural coarse aggregate [43]. The assumed transport distance of 100 km is further supported by Backes et al. [9], who applied the same transport distance for concrete constituents in a comparable environmental assessment of concrete mixtures.

For the concrete mixing process, a conservative electricity consumption based on the study of Dorer and Hahn [50] of 0.96 kWh per 1 m^3 was adopted. The corresponding electricity dataset represents the European market group for medium-voltage electricity.

For the minimum and maximum assessment of the GWP-t of concrete mixtures, a targeted review of available EPDs was conducted for the cement types considered in this study. This approach was selected because cement production is known to account for the majority of the environmental impacts of concrete mixtures, particularly with respect to GWP-t [51]. In total, 66 EPDs were identified for Portland cement, 30 EPDs for CEM III/A, and 20 EPDs for CEM III/B, all within the geographical scope of Europe.

To ensure a comparison on a consistent basis, conventional concrete mixtures corresponding to the compressive strength classes C12/15 to C60/70 were identified using the same EPD sources and within the same geographical scope as mentioned in Section 3.1. For each strength class, a range of EPDs was considered to represent variability in material formulation and production processes. This harmonised approach allows for a direct comparison between additively manufactured and conventional concrete systems under consistent environmental assumptions. The underlying datasets are documented and made available through a dedicated data publication [39]. Together, these data provide a comprehensive, regionally representative basis for capturing GWP-t variability and support a robust minimum- and maximum-value assessment.

3.2.3. Dynamic Winding Machine

The DWM described in Section 2.1 and seen in Figure 1 is analysed with 20 different ecoinvent datasets [39]. The primary machine components and the corresponding wearing parts were analysed. The system components considered include the DWM itself, the control cabinet, and the ventilation system. The primary structural and functional components of the DWM consist of aluminium, steel, motors, electrical components, and wood. The wear parts of the DWM comprise a plastic foil and a tube, both of which require replacement after every 100 printing hours. Fibre reinforcement production was measured at 30 m per hour. Since the DWM is a research-scale machine with no defined service life, environmental impacts were assessed for operational lifetimes of 5000 and 15,000 printing hours to account for potential usage variability.

3.3. Life Cycle Impact Assessment

The Life Cycle Impact Assessment (LCIA) was conducted according to DIN 15804 to ensure compatibility with EPDs and future studies, as it offers a construction-specific framework [34]. The impact categories are as follows: GWP-t; Global Warming Potential fossil (GWP-f); Global Warming Potential biogenic (GWP-b); Global Warming Potential land use (GWP-lu); Ozone Depletion Potential (ODP); Acidification Potential (AP); eutrophication potential - aquatic freshwater (EP-f); eutrophication potential - aquatic marine (EP-m); eutrophication potential - terrestrial (EP-t); Formation potential of tropospheric ozone photochemical oxidants (POCP); abiotic depletion potential for non-fossil resources (ADPE); abiotic depletion potential for fossil resources (ADPF); water use (WDP); total use of renewable primary energy resources (PERT); and total use of non-renewable primary energy resources (PENRT) are analysed in this study. The results of ADPE, ADPF, and WDP should be used with care as the uncertainties of the results are high and as there is limited experience with the indicator.

For the environmental assessment of the reinforcement materials (per 1 kg) and concrete mixtures (per 1 m^3), the full set of impact categories defined before is evaluated. For the analyses of reinforcement normalised by mechanical performance, the DWM, and the beam case study, the assessment is limited to the GWP-t. This simplification is chosen to enable a clear, streamlined comparison while reflecting the central importance of climate change as a dominant environmental concern [52].

4. Properties and Performance of FRP Reinforcements

The in-house produced rebars are characterised by determining their mechanical and geometric properties. On the one hand, structural design is carried out using representative values, while on the other hand, the actual environmental impact is determined.

4.1. Geometric Characteristics and Fibre Volume Fraction

Table 3 shows the average diameter and the fibre contents, including the corresponding standard deviations. The average BFRP rebar diameter of 4.13 mm is slightly above the average of GFRP with 3.97 mm, while the fibre volume content is lower (55.7 % compared to 60.8 %). The lower fibre volume content is therefore not caused by a smaller amount of fibres but by a higher resin content, i.e., due to less resin removal after the resin bath within the DWM. As the same process parameters were used for both materials while the fibre configuration differs (number of rovings, untwisted secondary basalt roving instead of twisted glass yarn), the present data do not allow separating the influence of the process setting from that of the fibre configuration. The evaluated diameter of each rebar is used for the following calculation of the specific mechanical properties.

Table 3. Average diameter, fibre volume content and fibre mass content with standard deviations of the produced GFRP and BFRP rebars.

	Diameter in mm	**Fibre Volume Content in %**	**Fibre Mass Content in %**
GFRP	3.97 ± 0.07	60.84 ± 2.01	77.96 ± 1.45
BFRP	4.13 ± 0.03	55.70 ± 0.99	75.19 ± 0.75

Figure 5 shows the surface profiling of the produced reinforcement strands. Visual inspections revealed that the cured GFRP rebars demonstrated superior and consistent surface quality (see Figure 5a). The BFRP rebars exhibit slightly less undulating surface (see Figure 5b) and a higher incidence of local defects. This includes occasional fraying (see Figure 5c) and waviness of the primary fibres (see Figure 5d). These observations are likely due to two main differences: the varying number of fibre rovings and the manual rewinding process before BFRP production to create additional spools. In particular, when preparing the additional rovings required, damage to the fibres and uneven tension as they enter the DWM cannot be ruled out. At the entrance of the machine, all rovings are guided into the resin bath. As the individual fibre strands are not separated, intersections may occur, leading to the observed effects later in the process.

The same process parameters (hysteresis brake, thread pitches) are selected for all production batches to ensure comparability of the rebars, which exhibit different surface structures. This effect can be caused by various factors. Firstly, the differing frictional properties of the fibres could influence the indentation behaviour. Reduced friction between the fibres in GFRP may facilitate easier filament displacement, allowing the tensioned thread to create deeper indentations. Secondly, the product types of the secondary fibres differ between the GFRP and BFRP rebars. For GFRP, a twisted yarn was used; for BFRP, an untwisted secondary basalt roving was available. This structural difference potentially contributes to the observed reduction in indentation depth.

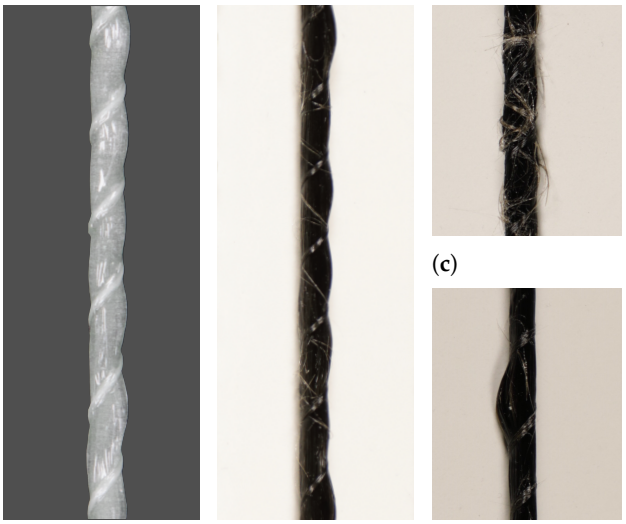


Figure 5. Comparison of BFRP to GFRP rebars and detected local defects (**a**) reference GFRP rebar, (**b**) average BFRP rebar, (**c**) fraying of the primary basalt fibres, (**d**) waviness of the primary fibres.

4.2. Experimental Tensile Performance

No invalid failures (failures within the sleeves or at the anchor mouth) were observed during the tensile tests. Only the test of sample B-02 was terminated prematurely before complete destruction and was excluded from all evaluations. This results in a sample size of 8 for GFRP and 7 for BFRP. The analysis of the stress–strain diagram in Figure 6 reveals that both fibre types share a comparable Young's modulus. This is indicated by a nearly identical initial stiffness at the start of the tests. The Young's modulus for the GFRP rebars ranges from 38.6 to 46.9 GPa with an average of approximately 42.5 GPa and a standard deviation of 3.1 GPa. For BFRP rebars the average is 45.4 GPa with a standard deviation of 1.9 GPa, ranging from 43.4 to 49.2 GPa. However, the produced rebars exhibit lower Young's moduli and higher elongation at break than commercial product information (see Schoeck Combar: 60 GPa [17]).

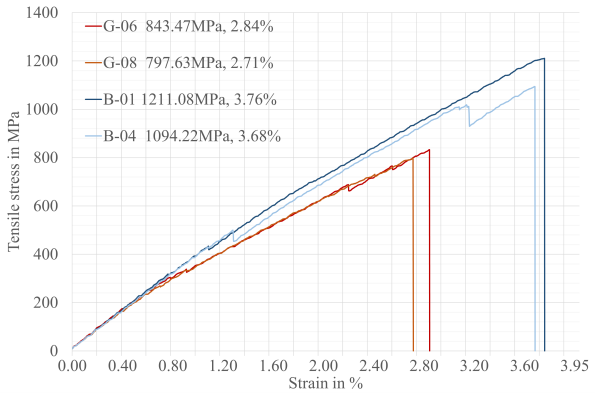


Figure 6. Comparison of tensile stress–strain-graphs of GFRP (G06, G08) and BFRP (B01, B04).

In the direct comparison, the BFRP rebars achieve higher tensile strengths than the E-CR-glass rebars, reaching values of 914.4 up to 1211.1 MPa and an average of 1106.3 MPa with a standard deviation of 85.7 MPa. The E-CR-glass fibre samples had an average tensile strength of 803.8 MPa (ranging from 757.8 to 877.9 MPa) with a standard deviation of 42.3 MPa, which is at most about 80% of the manufacturer's specifications of comparable commercial products (see Schoeck Combar: $>$1000 MPa [17]). It should be noted that

tensile tests performed in-house with commercially available rods also showed reduced tensile strength compared to the manufacturer's specifications. The tensile strengths were similar to those of specimens produced with the DWM [28].

The basalt samples also showed higher ductility with an approximate fracture strain of 3.5%. The GFRP rebars had a fracture strain of approximately 2.9% (see Figure 6). Overall, while the self-produced BFRP rebars fit the lower end of commercial standards, the glass fibre reinforcements fall short. The GFRP sample curves remain more consistently analogous until initial fibre failure at approximately 2.7% strain. Compared to this, BFRP shows abrupt stress drops in the diagram (cf. Figure 6 B-04 at 1.3% and 3.2% strain).

The differences within the curves can also be observed in different failure mechanisms for the two rebar types. Figure 7 shows their structural response under load, while GFRP leads to nearly orthogonal failure across the cross-section, and BFRP samples show a spreading along the fibre strands over their entire length. Splitting indicates that the fibre matrix interface or the inter-fibre matrix failed before the fibres reached their tensile capacity.

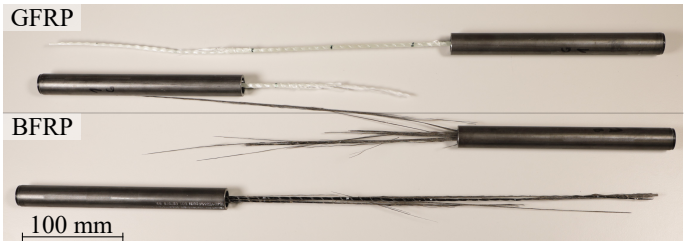


Figure 7. Failure differences between GFRP (top) and BFRP (bottom) rebars.

The tensile tests revealed no clear correlation between the visible, locally confined defects on the BFRP specimens and premature failure. Nevertheless, for future rewinding operations, the goal should be to implement automated rewinding or to ensure a sufficient number of rovings. Despite their differing surface properties, the BFRP specimens, just like the GFRP specimens, achieve around 80% of the tensile strength specified in commercially available reference data. Accordingly, the observed defects are not taken into account any further.

4.3. Assumed Long-Term Performance of Reinforcement Systems

The evaluation of the environmental impact of the manufactured reinforcements is based on a comparison of performance characteristics with two commercially available reinforcement types. Conventional steel rebars and pultruded high-performance CFRP rebars serve as the primary benchmarks. Their mechanical properties are derived from the standard definitions for B500B steel and technical data sheets provided by solidian [19].

A critical aspect of this study is the assessment of long-term environmental impacts. The long-term durability of FRP reinforcements is affected by mechanical loading (stress) and environmental influences (moisture, alkalinity, temperature) [53,54]. In particular, GFRP and BFRP rebars are subject to a reduction in tensile strength over their service life due to alkaline resistance or creep ruptures due to loads, which cause stress fractures. The resulting microcracks in the matrix enable chemical damage of the fibres [29,54–56]. These effects are much lower for CFRP rebars. Spelter et al. [57] could not evaluate a reduction factor for the mechanical properties of CFRP. Standard reduction factors provided by DIN-1992-1-1 [6] and the referencing DAfStb guideline [58] describe safety factors for accounting for long-term behaviour under given influencing factors. This information is not applicable to the materials in the assessment in this study, as the fabricated rebars are outside the standard's defined limits. Instead, this study investigates the potential of alternative

materials by aligning long-term performance assumptions with a commercially available benchmark, the commercially available Schöck Combar GFRP rebar [17]. For this product, the data sheet gives a short-term tensile strength of 1050 MPa and a characteristic long-term strength of 580 MPa for a service life of 100 years (5 % quantile, extrapolated from sustained-load tests in highly alkaline, moist concrete). The ratio of approximately 1.8 comprises the effects of sustained load and environment as well as the transition to the characteristic value of the benchmark. It was applied to the mean short-term strengths of the in-house rebars (804 MPa and 1106 MPa), yielding long-term strength of 445 MPa for GFRP. Due to their similar behaviour and no long-term data being available, the same assumptions were assumed for BFRP (610 MPa). For CFRP, reduction factors are much lower than the other fibre reinforcements [57]. This should ensure that a realistic investigation of FRP potential is conducted in accordance with industrial standards. The resulting assumed long-term properties and the origin of each material composition used for the following assessment are summarised in Table 4. These values do not yet include the partial safety factor, which is applied in the structural design (γ = 1.3, [58]).

Table 4. Scenario description of reinforcement materials, assumed long-term mechanical properties as design strength before partial safety factors and material composition sources.

Acronym	Material	Long-Term Tensile Strength in MPa	Young's Modulus in GPa	Material Composition Source
R1	B500B	500	200	DIN 488 [59]
R2	GFRP	445	42.5	This study
R3	BFRP	610	45.5	This study
R4	CFRP	1750	140	Backes et al. [9]

The mechanical properties of the reinforcement materials in this study differ from those reported in the literature, necessitating a comparison of their environmental-mechanical trade-offs. A notable divergence, such as Sbahieh et al. [22], lies in the assumed tensile strengths, which cite 1300 MPa (910 MPa design strength) for GFRP and 1900 MPa (1700 MPa design strength) for CFRP. The reinforcements produced via the DWM exhibit lower characteristic values (see Table 4 and Figure 6). This discrepancy can be attributed to inadequate fibre alignment and to the inherent variability of on-site automation compared to that of stationary pultruded products. By utilising these more conservative, in-house-measured tensile strengths, this study provides a realistic assessment of the environmental-mechanical trade-off for decentralised additive manufacturing processes, investigating the sustainability impact with materials that do not reach the theoretical limits of high-end commercial composites.

Consequently, this leads to a relatively conservative reduction in the reinforcement cross-section for FRP compared to steel, while other studies report significantly higher reduction factors; these are typically attributed to unconventional designs or a less prominent consideration of long-term strength degradation [60]. By utilising these more conservative, in-house-measured tensile strengths, this study provides a realistic assessment of the environmental-mechanical trade-off for decentralised additive manufacturing processes, demonstrating that sustainability impact can be lowered even with materials that do not reach the theoretical limits of high-end commercial composites.

5. E-LCA Results

5.1. Reinforcements

The cradle-to-gate E-LCA of the four reinforcement types per kilogram shows pronounced differences across all fifteen environmental impact categories (see Table 5), with

steel reinforcement consistently exhibiting the lowest environmental impacts. To ensure a streamlined and focused evaluation the dominance analysis of the reinforcement materials is limited to GWP-t. For steel, this study reports a GWP-t of 2.1 kg CO_2-eq per kg, which is in close agreement with literature values reported by Stoiber (2.3 kg CO_2-eq per kg) and Sbahieh (≈1.9 kg CO_2-eq per kg, when normalised to 1 kg), indicating comparatively low variability across studies. The slightly lower value reported by Sbahieh can be attributed to methodological differences, particularly the omission of transport processes, the use of a Qatar-specific geographical scope, and the application of GaBi background datasets, whereas the other studies are based on European datasets. The dominance analysis further shows that 99% of emissions originate from steel production (see Figure 8), while transport and manufacturing contribute only marginal shares, confirming steel as the lowest-impact reinforcement option on a mass basis.

Table 5. Environmental Life Cycle Assessment results for the reinforcement scenarios per kilogram reinforcement material.

Indicator	Unit	R1	R2	R3	R4
GWP-t	kg CO_2-eq	2.1	3.7	3.0	21.0
GWP-f	kg CO_2-eq	2.1	3.7	3.0	21.0
GWP-b	kg CO_2-eq	1.1×10^{-3}	4.7×10^{-3}	4.2×10^{-3}	2.2×10^{-2}
GWP-lu	kg CO_2-eq	1.2×10^{-3}	4.5×10^{-3}	3.7×10^{-3}	2.6×10^{-2}
ODP	kg CFC-11-eq	3.2×10^{-7}	3.4×10^{-6}	1.2×10^{-6}	5.7×10^{-6}
AP	molc H^+ eq	8.3×10^{-3}	2.4×10^{-2}	1.4×10^{-2}	1.2×10^{-1}
EP-f	kg P-eq	9.6×10^{-4}	1.8×10^{-3}	1.6×10^{-3}	8.0×10^{-3}
EP-m	kg N-eq	9.3×10^{-5}	1.9×10^{-4}	1.5×10^{-4}	1.9×10^{-3}
EP-t	molc N eq	2.0×10^{-2}	5.2×10^{-2}	3.3×10^{-2}	2.2×10^{-1}
POCP	kg NMVOC-eq	7.3×10^{-3}	1.6×10^{-2}	1.1×10^{-2}	6.8×10^{-2}
ADPE	kg Sb-eq	7.1×10^{-6}	4.1×10^{-4}	1.8×10^{-4}	2.5×10^{-4}
ADPF	MJ	21.5	52.4	47.1	263.4
WDP	m^3 world eq	0.9	1.3	1.0	4.8
PERT	MJ-eq	1.5	6.3	5.2	31.8
PENRT	MJ-eq	24.2	68.3	60.0	313.0

R2 and R3 show intermediate environmental burdens with total GWP-t values of 3.7 and 3.0 kg CO_2-eq, respectively. Their environmental profiles are shaped by the combined contributions of epoxy resin, fibre production, and production. For R2, the fibre accounts for 46% of its GWP-t and epoxy resin for 27%, while production contributes 26% and transport 1%. R3 displays a slightly different pattern: epoxy resin contributes 43%, fibre 24%, production 32% and transport 2% (see Figure 8). Minor deviations in the sum of contributions for R3 arise from the rounding of individual process contributions in the E-LCA results. Across the full set of indicators, both materials remain close to one another.

When compared with the literature, the results of this study fall within a similar range: for GFRP, values span from 2.1 kg CO_2-eq per kg [16] to approximately 2.7 kg CO_2-eq per kg (normalised to 1 kg reinforcement material [22]). The lower values reported by Sbahieh et al. [22] are again linked to simplified system boundaries and a non-European context using GaBi datasets, leading to differences in characterisation and emission factors. Pavlović et al. [21], based on ecoinvent APOS datasets, report higher values (≈4.84 kg CO_2-eq per metre for a 6 mm bar). However, direct comparability on a kg basis is limited due to missing information on material properties, preventing a reliable conversion. A similar trend is observed for BFRP, where literature values range from 1.6 kg CO_2-eq per kg [16] to 2.71 kg CO_2-eq per metre [21], with comparability again constrained by the use of length-based functional units and APOS background data.

R4 shows the highest environmental burdens across all impact categories. Its cradle-to-gate GWP-t is 21.0 kg CO_2-eq, more than six times higher than glass or basalt

fibre, and nearly ten times higher than steel. The majority of this impact (89%) originates from the carbon fibre itself, while epoxy resin contributes 6%, and the production of the reinforcement amounts to 5%. It should be noted that these results do not include "credit blend raw fibre" due to the lack of available inventory data. Consequently, the reported impacts for R4 may represent a conservative estimate, and the actual environmental burdens could be higher. This result is consistent with other European assessments, including Kromoser et al. [16] (21.5 kg CO_2-eq per kg) and Stoiber et al. [61] (19.7 kg CO_2-eq per kg), and exceeds the normalised result reported by Sbahieh et al. [22] (≈17.2 kg CO_2-eq per kg), which can again be explained by differences in system boundaries and the use of the GaBi database with regional datasets outside Europe.

Overall, while absolute GWP-t values vary across the literature, primarily due to differences in functional units, geographical scope, background datasets, and system boundaries, a consistent pattern emerges: CFRP exhibits the highest GWP-t, GFRP and BFRP intermediate values, and steel the lowest impacts on a mass basis. The classification of reinforcement materials in the literature is therefore typically limited to GWP-t, as it is the only impact category consistently assessed across all studies [16,21,22,61]. However, the comparison highlights that results should be interpreted in terms of relative trends rather than absolute values, given the strong influence of modelling assumptions.

Among the fifteen indicators (see Table 5), one outlier emerges for the glass fibre reinforcement: ADPE reaches 4.1×10^{-4} kg Sb-eq, more than twice as much as basalt fibre (1.8×10^{-4} kg) and substantially above carbon fibre (2.5×10^{-4} kg). Taken together, the results emphasise that the cradle-to-gate environmental performance per kilogram of reinforcement material varies strongly by material type. For this comparison value, steel offers the lowest-impact option, carbon fibre the highest-impact option, and glass and basalt fibres occupy an intermediate position, with modest variations across specific impact categories.

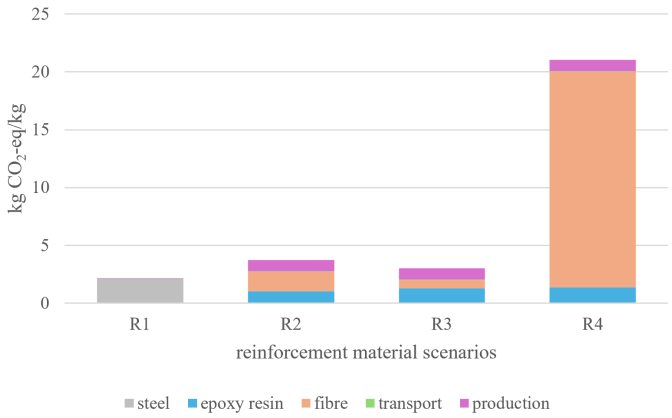


Figure 8. Dominance analysis of the four reinforcement scenarios, illustrating the influence of steel, epoxy resin, fibre, transport and production on total cradle-to-gate impacts.

Building on these findings, the GWP-t impacts associated with 1 kg of reinforcement were normalised by the tensile strength and Young's modulus of the respective materials, resulting in performance-based environmental impacts expressed as kg CO2-eq per MPA (impact per unit mechanical property) (see Table 6). Since the reinforcement materials differ in their mechanical properties (see Table 1), the normalisation allows the environmental impacts to be assessed not only per kilogram of material but also per unit of mechanical performance, thereby further highlighting the environmental differences between the reinforcement types on a functionally equivalent basis. R3 achieves the lowest GWP-t per unit of tensile strength, indicating the most favourable balance between carbon footprint

and load-carrying capacity. R1, while not the lowest in this category, still performs competitively and represents the next most carbon-efficient option relative to tensile strength. R2 occupies an intermediate position, whereas R4 exhibits a markedly higher GWP-t per unit tensile capacity, underscoring its substantially greater embodied carbon despite its high mechanical efficiency.

Table 6. Global Warming Potential total for life cycle phase A1 of 1 kg of the four reinforcement scenarios normalised by tensile strength and Young's Modulus.

Impact per Unit Mechanical Property	Unit	R1	R2	R3	R4
GWP-t/tensile strength	kg CO_2-eq/MPa	3.7×10^{-3}	6.1×10^{-3}	3.4×10^{-3}	1.14×10^{-2}
GWP-t/Young's modulus	kg CO_2-eq/MPa	9×10^{-6}	6.4×10^{-5}	4.6×10^{-5}	1.43×10^{-4}

When normalised by Young's Modulus, the ranking shifts slightly: steel reinforcement becomes the most carbon-efficient option per unit, while basalt and glass fibres fall into a moderate range. Carbon fibre again shows the highest GWP-t per Young's Modulus, exceeding all other reinforcement types by a significant margin. Together, these results demonstrate that the environmental efficiency of reinforcement materials depends not only on their absolute impact but also on how effectively they translate embodied emissions into mechanical performance. Basalt fibre offers the best carbon-to-strength efficiency, steel provides the best carbon-to-stiffness balance, and carbon fibre consistently performs the poorest under both metrics due to its high A1-stage emissions relative to its mechanical properties.

5.2. Concrete Mixtures

The environmental results of the ten additive manufacturing concrete mixtures (see Table 7) show substantial variation, driven by differences in cement content and aggregate composition. Across all mixtures, the A1 stage (raw material production) accounts for the vast majority of the total GWP-t [39], while the A2 (transport) and A3 (manufacturing) stages contribute only marginally, and this dominance is reflected consistently across all mixtures. Across all mixtures, cement is the dominant contributor, accounting for 66–86% of total GWP-t per m^3. The results demonstrate that environmental burdens are strongly governed by the amount and type of cement used, while the influence of aggregates, admixtures, transport and production remains comparatively minor.

The GWP-t results show a pronounced differentiation between the mixtures. The Portland-cement-rich mixtures C1, C2 and C3 exhibit the highest climate impacts, exceeding 568–696 kg CO_2-eq per m^3. These mixtures contain the largest proportions of CEM I (ranging from 550 to 700 kg/m^3), which directly reflects their high contribution to the GWP-t with well over 80% of their embodied emissions. These mixtures also produce the highest values in most other impact categories. C1 and C3 are also influenced by the usage of PVAf and carboxy cellulose, contributing together 9% and 10% for C1 and C3, which is quite high in perspective of the overall sum of the GWP-t. C2 has such high amounts of admixtures that they contribute 8% to the overall GWP-t.

The mixtures C4, C5, and C6, each containing approximately 371–376 kg of Portland cement in combination with ggbfs, exhibit substantially lower GWP-t values (384–392 kg CO_2-eq/m^3) than the Portland-cement-dominated mixtures. Although cement still accounts for more than 80% of their total GWP-t, the strategic reduction of clinker and the partial substitution with ggbfs significantly decrease the overall climate impact. Ggbfs itself

contributes roughly 9% to the total GWP-t in all three mixtures. Moreover, the use of sand, gravel and recycled gravel instead of silica sand (as used in C1 - C3) slightly reduces the impact intensity, since silica sand exhibits a higher footprint in several categories.

Table 7. Environmental impact indicators per m³ for the ten additive manufacturing concrete mixtures (C1–C10) across all analysed E-LCA impact categories.

Indicator	Unit	C1	C2	C3	C4	C5	C6	C7	C8	C9	C10
GWP-t	kg CO_2-eq	696	623	568	392	387	384	429	191	469	334
GWP-f	kg CO_2-eq	696	622	568	392	387	384	429	187	469	334
GWP-b	kg CO_2-eq	0.03	1.03	0.01	0.10	0.10	0.10	0.08	3.52	0.05	0.19
GWP-lu	kg CO_2-eq	0.15	0.12	0.13	0.13	0.13	0.13	0.11	0.07	0.22	0.16
ODP	kg CFC-11-eq $\times 10^{-5}$	4.6	4.3	4.0	3.7	3.7	3.7	4.7	2.9	5.0	4.4
AP	molc H^+ eq	1.67	1.49	1.41	1.10	1.07	1.06	0.99	0.52	1.49	1.33
EP-f	kg P-eq	0.08	0.07	0.07	0.05	0.05	0.05	0.05	0.03	0.07	0.05
EP-m	kg N-eq $\times 10^{-2}$	3.6	2.9	3.4	0.43	0.42	0.41	0.47	0.47	3.5	0.83
EP-t	molc N eq	5.02	4.59	4.18	2.93	2.89	2.86	2.80	1.50	3.72	3.47
POCP	kg NMVOC-eq	1.50	1.35	1.26	0.90	0.88	0.87	0.96	0.50	1.18	1.02
ADPE	kg Sb-eq $\times 10^{-4}$	9.2	6.5	7.8	150	150	140	380	5.2	10	7.0
ADPF	MJ	3299	3559	2858	1955	1896	1886	2758	1284	2998	2791
WDP	m^3 world eq	162	128	158	142	140	117	162	43	146	93
PERT	MJ-eq	410	229	342	161	158	153	141	142	423	187
PENRT	MJ-eq	3895	4024	3341	2338	2271	2255	3193	1509	3541	3076

Mixtures C7 achieves further reductions in clinker demand by lowering the Portland cement content to 331 kg/m³ and substituting substantial portions with calcined clay and limestone. As a result, CEM I contributes only 66% to the global GWP-t, while calcined clay accounts for 21%. Admixtures contribute an additional 7% to the climate impact due to their elevated relative share within the now-reduced overall GWP-t, while C7 performs well across most impact categories, it stands out as an outlier in ADPE, where it exhibits the highest value among all mixtures, as well as in water use, where it ranks at the upper end together with C1. C7 also shows the second highest value in ODP, following C9.

Mixture C9, which is based on CEM III/A, contains 700 kg/m³ of binder and therefore shows a higher GWP-t than mixtures C4–C8, despite their reliance on CEM I, because these mixtures use substantially lower amounts of it. In C9, cement accounts for 80% of its total GWP-t, while additives account for 14% due to their comparatively higher proportional share in the mixture. C9 also presents several outlier behaviours, as it shows the highest ODP and GWP-lu among all mixtures and the second-highest EP-m value.

Mixture C10, based on CEM III/B with a total cementitious material content of approximately 400 kg/m³, achieves the second-lowest GWP-t in the dataset while simultaneously delivering the lowest compressive strength class (C12/15). Cement accounts for 44% of total GWP-t, with CSA cement accounting for an additional 39%. Silica sand contributes 8%, and admixtures about 3%. The strong reduction in clinker content, together with the high proportion of ggbfs and CSA cement, results in a substantially improved climate and resource profile across most categories.

The elevated ADPE value of mixture C7 is mainly caused by the comparatively high dosage of VMA (2.0 kg/m³), while mixtures C4, C5 and C6 also show comparatively elevated ADPE values due to the inclusion of VMA; the lower admixture dosage (0.74–0.75 kg/m³) results in substantially smaller contributions than C7. However, as outlined in Section 3.3, ADPE results should be interpreted with caution due to the high uncertainties associated with this indicator and the still limited experience in its application within E-LCA studies.

The results for mixtures C2, C8, and C10 are subject to additional uncertainty because product-specific inventory data for the incorporated defoamer and stabiliser were unavail-

able, and their potential contributions to individual impact categories could therefore not be robustly quantified.

Overall, integrating the A1, A2, and A3 separation confirms that A1 overwhelmingly drives the total GWP-t and that the environmental profiles of the mixtures are shaped primarily by the quantity and type of cement and aggregate materials used. Mixtures with lower binder contents and fewer high-impact speciality constituents perform best, demonstrating that substantial impact reductions can be achieved through careful material selection, without necessarily compromising compressive strength requirements. This aligns with Scrivener et al. [51], who identify clinker content and binder intensity as the main drivers of concrete's environmental impact and highlight clinker substitution and optimised aggregate packing as key strategies for reducing CO_2 emissions.

The comparison of AM and conventional manufacturing (CM) concrete mixtures across compressive strength classes shows a clear divergence in absolute GWP-t values (see Figure 9).

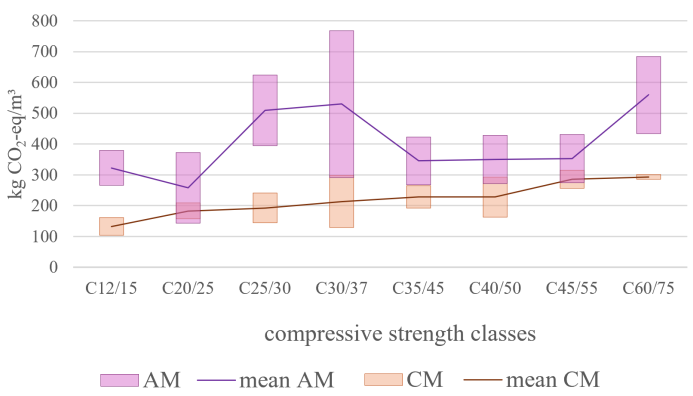


Figure 9. Comparison of GWP-t ranges across compressive strength classes for CM and AM concrete.

AM mixtures exhibit consistently higher GWP-t values within each strength class, with mean values increasing notably toward higher strength classes. In contrast, CM mixtures show a more gradual increase in GWP-t. This divergence can be attributed to the more complex mix design requirements of AM concrete, which must satisfy conflicting rheological constraints, combining sufficient flowability for extrusion with rapid stiffness and buildability to support subsequent layers [62]. These requirements lead to more material-intensive formulations, making AM mixtures particularly sensitive to mix design, especially at higher strength classes where GWP-t levels peak.

5.3. Dynamic Fibre Winding

The results of the DWM analysis (see Figure 10) show a clear reduction in the environmental burden of the DWM as service life increases. The GWP-t per hour of printing time steadily declines from around 0.70 kg CO_2-eq at shorter service-life assumptions to below 0.25 kg CO_2-eq at the upper end. This behaviour reflects the amortisation of the machine's fixed upstream and operational impacts over a larger number of productive hours. When this hourly impact is normalised by the amount of fibre reinforcement the system can produce per hour, the resulting GWP-t per metre of produced reinforcement remains very low with 0.023 kg CO_2-eq and shows only a slight downward trend. This indicates that while a longer service life significantly reduces the DWM's hourly environmental intensity, the impact allocated per metre of reinforcement is inherently small due to high production efficiency of the process. Overall, these findings demonstrate that the carbon efficiency of the DWM system improves markedly with increasing service life.

A comparison of the reinforcement production processes highlights noticeable differences in environmental performance. The DWM process evaluated in this study, including the associated electricity consumption, results in emissions of 0.96 kg CO_2-eq per kg of reinforcement, assuming a service life of 10,000 operating hours for the machine. This value is higher than the 0.57 kg CO_2-eq per kg reported for conventional pultrusion processes [63]. The dominant production contribution within the DWM process originates from the machine depreciation (≈70%), while only about 30% of the emissions stem from the actual energy consumption during operation (see Figure 8). This indicates that the environmental impact of the DWM is largely driven by capital equipment allocation rather than process energy demand.

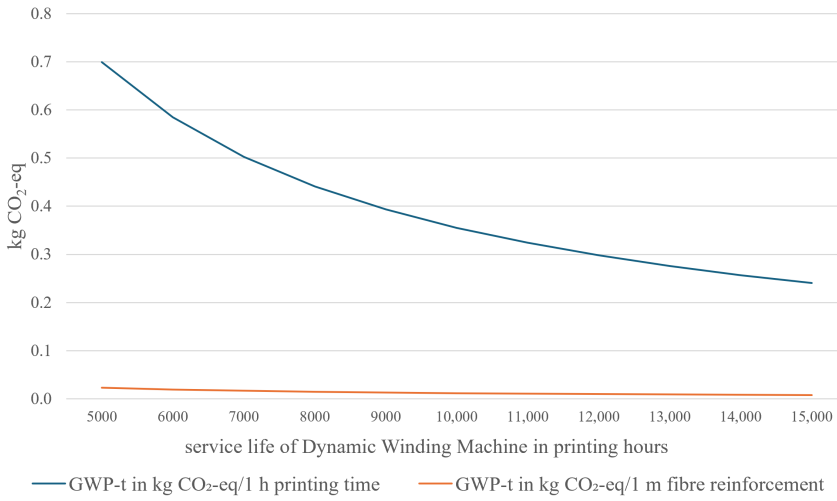


Figure 10. GWP-t impact of the DWM per fabrication hour and 1 m of fibre reinforcement depending on the service life.

5.4. Beam Case Study

Table 8 shows the cross-section dimensions for each concrete, derived based on the requirements for steel reinforcement under the conditions described in Section 3.1. The FRP-reinforced cross-sections are reduced in height by 5 mm. As the study compares reinforcement materials for a generic beam and not for a specific structure, no exposure class was verified; instead, the lowest exposure class XC1 (service life of 100 years, structural class S2 was adopted as the reference condition. For these conditions, the minimum cover according to DIN EN 1992-1-1 [6] and the DAfStb guideline [58] differs by 5 mm between steel and non-metallic reinforcement. The guideline value for FRP reinforcements is independent of the concrete strength class and applies to bar diameters below 16 mm, so the reduction was applied uniformly. The results are therefore valid for this reference condition, and the achievable reduction in other exposure classes has to be determined separately.

For each cross-section, the structural simulations were used to determine the required quantities of longitudinal and stirrup reinforcement based on the applied loads. These results served as the basis for calculating the net concrete volume, obtained by subtracting the reinforcement volume from the gross cross-section. In parallel, the corresponding reinforcement mass was derived for each configuration. The resulting geometrical and material quantities are summarised in Table 9. C12/15 shows increased values for GFRP and BFRP compared with the remaining reinforcement quantities, which is caused by an increased longitudinal reinforcement mass. As the calculations were conducted consistently across all designs, these values reflect the interaction between low concrete strength and FRP reinforcement mechanics. Specifically, this sharp increase may be governed by the structural design requirements for SLS stiffness and cracking control requirements,

rather than ultimate load-bearing capacity alone. Further discussion of these constraints is provided in Section 6.2. However, they should be regarded with caution.

Table 8. Conventional beam dimensions for the calculation of the minimum amount of reinforcement according to the concrete mixture properties.

Concrete	Height in m	Width in m
C12/15	0.436	0.218
C20/25	0.421	0.210
C25/30	0.412	0.206
C30/37	0.400	0.200
C35/45	0.390	0.195
C40/50	0.380	0.190
C45/55	0.369	0.185
C60/75	0.342	0.171

Table 9. Reinforcement mass ($m_{R\{1..4\}}$) and required concrete volume ($V_{\text{concrete},R\{1..4\}}$) for each analysed compressive strength class needed to meet the structural requirements of the beam.

	C12/15	C20/25	C25/30	C30/37	C35/45	C40/50	C45/55	C60/76
m_{R1} [kg]	19.08	18.94	18.86	18.74	18.65	20.04	19.89	21.06
$V_{\text{concrete},R1}$ [m^3]	0.38	0.35	0.34	0.32	0.30	0.29	0.27	0.23
m_{R2} [kg]	10.19	6.58	6.53	6.46	6.80	6.73	7.05	7.20
$V_{\text{concrete},R2}$ [m^3]	0.33	0.31	0.29	0.28	0.26	0.25	0.23	0.20
m_{R3} [kg]	9.31	5.29	5.69	5.63	5.58	5.93	5.87	5.30
$V_{\text{concrete},R3}$ [m^3]	0.33	0.31	0.30	0.28	0.26	0.25	0.23	0.20
m_{R4} [kg]	2.80	2.47	2.45	2.43	2.41	2.69	2.66	2.59
$V_{\text{concrete},R4}$ [m^3]	0.34	0.31	0.30	0.28	0.26	0.25	0.23	0.20

The GWP-t of the optimised beam exhibits considerable variation across both reinforcement types and concrete strength classes, as illustrated in Figure 11. This variability reflects the combined influence of the intrinsic environmental burdens of the constituent materials and the differing structural performance requirements associated with each compressive strength class. In general, CM concrete solutions demonstrate lower GWP-t values compared to AM concretes, with the notable exception of the C20/25 class, where the minimum GWP-t values of AM beams fall below those of CM beams. This behaviour is consistent with the trends observed in Figure 9, where the minimum environmental impacts of CM concrete are lower than their AM counterparts for the remaining strength classes. Regarding reinforcement strategies, R2 and R3 consistently yield the lowest GWP-t values for both CM and AM beams, except in the case of the C12/25 class, where R1 achieves the lowest GWP-t for CM concrete. R2 and R3 exhibit highly comparable environmental performance, with substantial overlap in both minimum and maximum GWP-t values, and neither material consistently outperforms the other. These fibre-based reinforcements, therefore, form a clear intermediate category, significantly outperforming R4. R4, despite its high mechanical efficiency, results in the highest GWP-t values at the beam level across all strength classes, particularly when considering minimum values. The similarity between Figures 9 and 11 further indicates that the environmental impact of the beam is strongly governed by the concrete component. This suggests that the contribution of the concrete mixture dominates the overall GWP-t while reinforcement plays a secondary, though still significant, role. Overall, the results demonstrate that the environmental performance of optimised beams is governed by the interaction between reinforcement type, concrete

composition, and required strength class. R2 and R3 exhibit, on average, in most strength classes, 13% and 15% lower GWP-t values than R1, whereas R4 consistently results in the highest embodied carbon. These findings underline the importance of integrated material selection strategies, in which both concrete mix design and reinforcement choice are aligned with sustainability objectives.

The interpretation of these results must be considered in the context of existing E-LCA studies, where the performance of FRP and steel reinforcement is strongly influenced by environmental conditions and design assumptions. Studies by Sbahieh et al. [22], Dong et al. [23], Pavlović et al. [21], and Steckbauer et al. [60] frequently report superior environmental performance for FRP-reinforced systems. However, these findings are typically based on specific design strategies. A key parameter in this context is the treatment of concrete cover. Optimisation-based approaches, such as Dong et al. [23], consider aggressive environments and exploit the corrosion resistance of FRP to significantly reduce cover thickness, enabling slender cross-sections and substantial concrete savings. In contrast, validation approaches (e.g., Pavlović et al. [21]) maintain identical geometries to isolate mechanical effects. The present study bridges these approaches by ensuring structural equivalence while allowing geometric adaptation to material properties. Unlike optimisation-focused studies, it does not assume aggressive exposure conditions or extreme cover reductions. Instead, it demonstrates that GFRP and BFRP reinforcements remain environmentally competitive with steel even under conventional design conditions, where the influence of corrosion resistance is less pronounced.

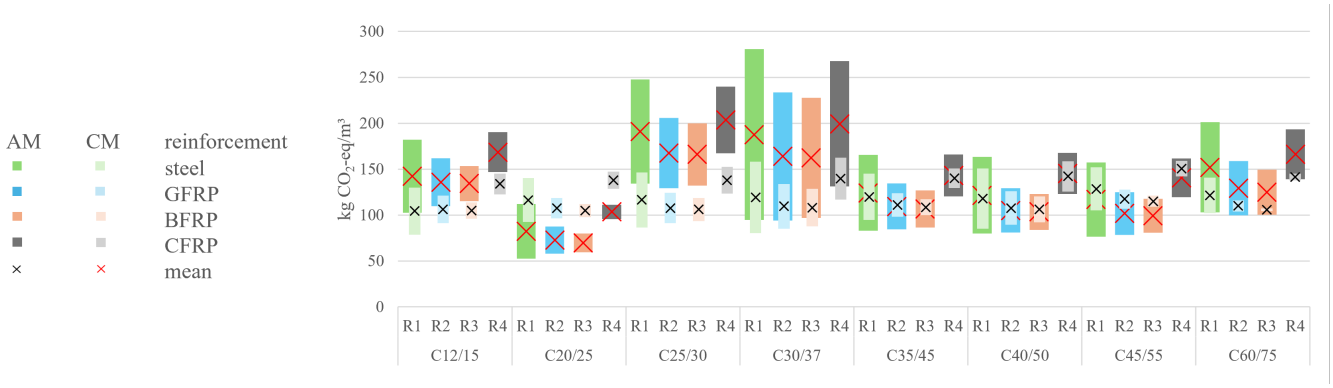


Figure 11. Range of GWP-t values for the optimised beam case study across all reinforcement types (R1–R4) and concrete compressive strength classes (C12/15–C60/75).

For a more detailed assessment of the relative contributions of concrete and reinforcement to the beam's GWP-t, the strength class C20/25 with the AM mixture C8 was selected (see Figure 12). For steel reinforcement, the C20/25 scenario shows that, even though steel requires the largest reinforcement mass, the contribution of the reinforcement to the GWP-t remains very small in the minimum case, accounting for only 6% of the beam's overall impact. The remaining 94% originates from the concrete. In the maximum case, however, the share of the reinforcement increases substantially to 36%, leading to GWP-t values that exceed the maximum scenarios of R2 and R3. Notably, even the minimum reinforcement-related impact of the R4 scenario remains higher than the maximum reinforcement contribution of steel. For the R2 and R3 scenarios, the reinforcement accounts for 21–28% of the GWP-t across the minimum and maximum configurations, placing both materials in a narrow and consistent mid-range. The highest reinforcement shares occur in the R4 scenario, where reinforcement contributes 48–52% of the GWP-t, making R4 the CFRP the dominant environmental driver in this configuration despite its low mass requirement. These results substantiate the earlier observation that the concrete component

exerts a predominant influence on the overall GWP-t of the beam, although the choice of reinforcement material can substantially alter the relative contribution and, in some cases, the total environmental impact.

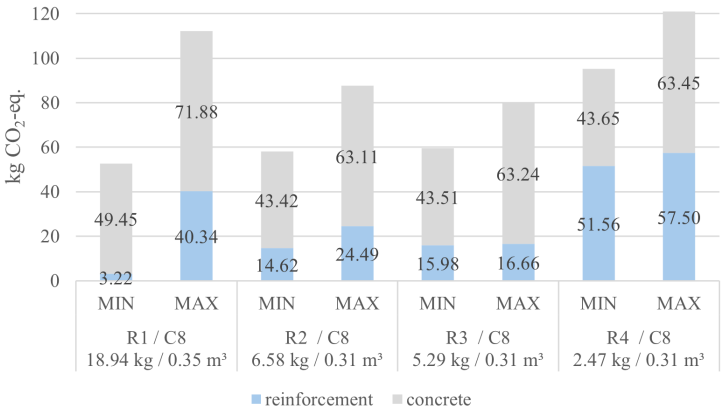


Figure 12. GWP-t distribution for the beam between reinforcement and AM concrete for the compressive strength class C20/25 (C8).

6. Discussion

6.1. Reinforcement and Production

The investigations and findings on environmental impact in this paper are based on in-house-produced reinforcements with a DWM. The production method is a research objective for the fabrication of free-formable reinforcement strands. The tensile tests revealed average tensile strengths of 1106 ± 86 MPa for BFRP and 804 ± 42 MPa for GFRP. Similarly, the Young's moduli were determined to be 45.4 GPa and 42.5 GPa. Both the strength and stiffness values of the specimens are lower than the specifications provided by manufacturers of commercially available pultruded rebars. This discrepancy is primarily attributable to the measured fibre volume fraction of 55–60%. Future investigations should include void content tests to determine whether these differences can be attributed to higher void contents. Furthermore, the observed failure modes suggest that the manufacturing process offers potential for further refinement. The mechanical properties used in this study were determined on rebar specimens that contained the observed manufacturing defects and scatter, so their influence is included in the tested values for the investigated rebars and beam case study. With increasing rebar length and component size, the probability of critical defects increases, exerting a stronger influence on strength and, consequently, on the required reinforcement quantity and the LCA results. Scaling up the technology, therefore, requires further tests and evaluations on larger reinforcement structures to derive new characteristic values and verify them.

The axial failure at BFRP rebars may be caused by uneven pre-tensioning of the rovings during production, which generates internal shear forces and leads to subsequent sliding between fibre strands. The failure of individual fibre bundles is thought to be the cause of the abrupt drops in the stress–strain curve. Other possible contributions are incomplete impregnation of the rovings in the resin bath, local defects, a lower fibre volume fraction and the interfacial shear strength (IFSS) between the basalt fibres and the epoxy matrix, which depends on the fibre sizing and its compatibility with the MGS RIMR 426 system. IFSS was not measured in this study, so this explanation remains a hypothesis.

Future iterations of the DWM production are expected to yield higher fibre compaction, better guidance and consistent pre-tensioning, leading to mechanical properties more closely aligned with industrial standards. The fibre volume content of the BFRP rebars

(55.7 %) is in this comparison lower than that of the GFRP rebars (60.8 %) at a comparable fibre cross-section, so that an adjusted resin removal is expected to slightly increase the strength and stiffness related to the gross cross-section. The influence of a more uniform fibre alignment and pre-tensioning on the structural performance could not be quantified with the present data and has to be investigated in future production series with controlled roving tension. However, Rothe et al. [28] demonstrated through direct comparison that the tensile strength of these self-produced GFRP strands is comparable to that of commercial rebars. To ensure maximum transparency and design reliability, these self-verified values were used and adopted for the structural design in this work.

The stirrup strength is based on a factor transferred from a commercial product (see Section 3.1). The corner strength of continuously wound fibres may differ from that of factory-bent rebars, since it depends on the bend radius, the fibre type and the production method. The behaviour of DWM reinforcement at bent sections is therefore an interesting subject for further research, e.g., through tensile tests on bent specimens with varying bend radii.

The evaluation of the sustainability impact of FRP reinforcements focuses on fibre types, while the matrix system was kept constant to ensure comparability. This isolated approach allows for a direct assessment of fibre influence but excludes potential ecological optimisations through alternative or bio-based resin systems. Integrating such matrix systems could further improve the environmental performance of FRP reinforcements relative to the steel-reinforced benchmark beyond the results presented.

6.2. Simulation

The comparative analysis is based on a steel-reinforced concrete beam baseline, against which various AM mixtures and FRP reinforcement types are benchmarked. To ensure a technically rigorous comparison, an iterative Python-based optimisation was employed. This approach adjusted the geometry based on the specific compressive strengths and Young's Moduli of the concrete mixtures. Compared to a closed-form governing-criterion solution, obtained by enforcing exact equivalence with respect to whichever criterion is more restrictive, the weighted approach used in this study systematically unsatisfies the governing criterion rather than approaching it as w increases. For concrete classes close to the reference class C30/37, this deviation remains below 10 %, and can reasonably be regarded as negligible. For the marginal classes, this deviation is substantial, reflecting a shift in the governing criterion from load-bearing capacity to stiffness as concrete strength increases, since the characteristic compression strength varies more strongly across the investigated classes than the Young's modulus. This confirms that a single-criterion assessment would not adequately capture the governing constraint across the full range of concrete classes. Given these limitations, the presented cross-section design should be seen as a comparative baseline that provides a consistent, reproducible basis for comparing concrete classes under simplified yet physically motivated proxy criteria, prior to the detailed reinforcement design carried out in SOFiSTiK. The proxy criteria are exclusively to define a common concrete cross-section for each concrete class. Within this scope, the method captures the two most relevant structural design aspects, flexural load-bearing capacity and stiffness, while deliberately trading a degree of criterion-specific precision for a balanced, extensible formulation. The reinforcement quantities entering the life cycle assessment therefore result from a design based on the actual mechanics of each material, not from the proxy criteria. The results are therefore valid as a comparison under equal geometric boundary conditions and should not be read as a design-ready optimisation. Results for classes at the margins of the investigated range should accordingly be interpreted with caution. Furthermore, the concrete cover was reduced for the FRP variants in compliance

with DAfStb guideline for non-metallic reinforcements [58] and DIN 1992-1-1 [6], reflecting the material's inherent corrosion resistance. However, it must be noted that this study utilised conventional structural assumptions as a baseline for the optimisation process, while the current calculation uses a mechanically driven adaptation to meet structural comparability of the beam cross-sections, it does not yet account for an ecologically driven optimisation. Incorporating environmental impact as a direct variable into the iterative process could yield significantly different beam geometries and reinforcement ratios for each material type. Furthermore, to fully exploit the fibre potential of the DWM process, future designs could transcend conventional reinforcement layouts. For instance, dissolving traditional stirrup configurations in favour of continuous, multi-axial longitudinal layouts could further enhance structural efficiency and reduce material consumption. Consequently, the results presented here represent a conservative benchmark that could be further improved by transitioning from conventional reinforcement logic to a truly fibre-optimised design approach.

6.3. Beam Case Study

Although the potential for material optimisation may be higher in specialised applications or complex structural components, a standardised beam element was selected as the primary benchmark to ensure a transparent, generalisable analysis. This fundamental case study isolates the environmental and mechanical performance of in-house-manufactured FRP reinforcements from the effects of intricate geometries, establishing a reliable baseline for comparison with conventional steel. However, it is important to note that these results still represent a conservative application of 3D-printing technology, while the cross-sections were optimised for material properties, the simulation remains bound by traditional prismatic beam geometries.

The applicability of the present findings to other structural systems must be considered with caution. The analysed case study focuses on relatively short-span, non-prestressed beams, and the environmental ranking of reinforcement systems may change for larger span elements, which typically require substantially different structural concepts, higher reinforcement ratios, prestressing, or alternative cross-section geometries. Moreover, the conclusions derived here for load-bearing beams cannot be directly transferred to non-structural elements, such as facade panels. In facade applications, textile- or fibre-reinforced concrete systems have been shown to outperform steel-reinforced solutions from an environmental perspective, as demonstrated by Laiblova et al. [64], primarily due to their significantly reduced concrete cover requirements and lower material volumes. Accordingly, any assessment of environmental sustainability requires a careful application-specific evaluation, as conclusions cannot be generalised across different structural functions, geometries, and design requirements.

6.4. Environmental Life Cycle Assessment

While the present study focuses exclusively on cradle-to-gate impacts, it is important to acknowledge that a complete environmental assessment of reinforced concrete structures would also need to consider the use phase and end-of-life (EoL) stages. Parameters such as durability, maintenance requirements, service life extension, and potential reuse or recycling pathways may substantially influence the total life-cycle impact and, in some cases, alter the relative performance of different reinforcement systems. For FRP materials in particular, the EoL phase remains highly uncertain. Multiple EoL pathways are theoretically possible for composite materials, including landfill, incineration, mechanical recycling, and various forms of downcycling. However, the lack of established and widely implemented industrial processes, combined with limited empirical field data for FRP-reinforced concrete

structures, makes it difficult to define representative and robust Module C and D scenarios without introducing significant uncertainty into the assessment [21]. Dedicated research on EoL aspects of CFRP concrete has been conducted by Backes et al. [65], who demonstrated that end-of-life assumptions can have a considerable impact on the overall environmental profile of carbon-reinforced concrete components. Their work illustrates both the potential importance of EoL modelling and the sensitivity of results to assumptions on recycling routes, energy recovery, and allocation procedures. However, these findings are currently limited to CFRP-based systems and cannot be directly transferred to glass- or basalt-fibre reinforcement due to differences in material composition, recycling potential, and technological maturity. In contrast, steel reinforcement benefits from well-established recycling routes and efficient recovery from demolished concrete. Consequently, the relative environmental performance of GFRP and BFRP compared to steel may change when EoL processes and associated recycling credits are incorporated into the assessment. Given these uncertainties, extending the present assessment to include use-phase and EoL stages would require a comprehensive set of well-founded assumptions that cannot yet be supported by practice or reliable data for all reinforcement types investigated.

7. Conclusions

A key finding of this comparative E-LCA is that GFRP and BFRP reinforcements manufactured in-house using the DWM can achieve GWP-t levels comparable to conventional steel reinforcement while providing sufficient mechanical performance for the beam case study.

The mechanical basis is supported by tensile tests yielding average strengths of 1106 MPa for BFRP and 804 MPa for GFRP, with Young's moduli of 45.4 GPa and 42.5 GPa, respectively. Although these values are lower than industrial pultrusion standards, primarily due to a moderate fibre volume fraction (55 – 60%), the use of these self-verified data points ensures a transparent and reliable structural design. Observed failure modes and tensile curve progressions identify clear technical pathways for further refining the DWM, specifically in fibre compaction and alignment.

At the structural level, GFRP and BFRP achieved GWP-t values comparable to, and in some scenarios lower than, those of conventional steel reinforcement, with GWP-t reduced by up to 13% and 15%, respectively. These results highlight the potential of the DWM wound reinforcement as a sustainable alternative for concrete reinforcement. While CFRP exhibits superior mechanical properties, its environmental burden remains significantly higher compared to the three alternative analysed materials.

Beyond the reinforcement material, concrete mix design remained the dominant driver of environmental impacts in the beam case study, with the concrete mixture contributing more than 50% of the GWP-t across both the minimum and maximum scenarios, exceeding the contribution of the reinforcement materials.

The results further indicate that free-form reinforcement produced by DWM can enable environmental benefits even when using materials with lower mechanical performance. However, material substitution alone is insufficient to fully exploit this potential. Meaningful environmental improvements require the combined optimisation of reinforcement design, structural geometry, and material selection, highlighting the importance of integrated design approaches rather than simple one-to-one substitution strategies.

The findings substantiate that, for the selected structural component analysed in this study, transitioning to automated FRP fabrication provides a measurably more sustainable solution compared to conventional steel reinforcement. By fully embracing the free-form potential of this approach, future concrete components can be geometrically

tailored to drastically reduce material consumption and mitigate the high carbon intensity of the sector.

Author Contributions: Conceptualization, S.V.A., P.T., C.H., and C.T.; methodology, S.V.A. and P.T.; software, S.V.A. and P.T.; validation, S.V.A. and P.T.; formal analysis, S.V.A., P.T., and D.D.; investigation, S.V.A., P.T., and D.D.; resources, C.H. and C.T.; data curation, S.V.A., P.T., and T.R.; writing—original draft preparation, S.V.A. and P.T.; writing—review and editing, S.V.A., P.T., T.R., C.H., and C.T.; visualization, S.V.A., P.T., and D.D.; supervision, C.H. and C.T.; project administration, C.H. and C.T.; funding acquisition, C.H. and C.T. All authors have read and agreed to the published version of the manuscript.

Funding: This research was funded by the Deutsche Forschungsgemeinschaft (DFG, German Research Foundation)—Project Number 414265976—TRR277. The authors thank the DFG for the sup- port within Transregio 277—Additive Manufacturing Construction (Projects A05, C09). This publication was funded by Ostbayerische Technische Hochschule Regensburg, whose support is greatly appreciated.

Institutional Review Board Statement: Not applicable.

Informed Consent Statement: Not applicable.

Data Availability Statement: The original data presented in the study are openly available in Zenodo at https://zenodo.org/doi/10.5281/zenodo.19973658 (accessed on 26 May 2026) and https://zenodo.org/doi/10.5281/zenodo.20395834 (accessed on 4 May 2026).

Conflicts of Interest: The authors declare no conflicts of interest.

Abbreviations

The following abbreviations are used in this manuscript:

ADPE	abiotic depletion potential for non-fossil resources
ADPF	abiotic depletion potential for fossil resources
AMC	Additive Manufacturing in Construction
AM	Additive Manufacturing
AP	Acidification Potential
AR	alkaline-resistant
BFRP	basalt fibre-reinforced polymers
cc	calcined clay
CFRP	carbon fibre-reinforced polymers
CM	Conventional Manufacturing
CSA	Calcium Sulfoaluminate cement
d	defoamer
DWM	Dynamic Winding Machine
E-CR	electric corrosion-resistant
E-LCA	Environmental Life Cycle Assessment
EoL	End-of-Life
EPD	Environmental Product Declaration
EP-f	eutrophication potential–aquatic freshwater
EP-m	eutrophication potential–aquatic marine
EP-t	eutrophication potential–terrestrial
fa	fly ash
FRP	fibre-reinforced polymer
GFRP	glass fibre-reinforced polymers
ggbfs	ground granulated blast furnace slag
GWP-b	Global Warming Potential biogenic
GWP-f	Global Warming Potential fossil
GWP-lu	Global Warming Potential land use

GWP-t	Global Warming Potential total
l	limestone
LCIA	Life Cycle Impact Assessment
MC	Methylcellulose
ODP	Ozone Depletion Potential
PENRT	total use of non-renewable primary energy resources
PERT	total use of renewable primary energy resources
POCP	Formation potential of tropospheric ozone photochemical oxidants
p	plasticiser
PVAf	Polyvinyl Alcohol fibre
r	retarder
rca	recycled coarse aggregate
s	sand
sa	set accelerator
SCMs	Supplementary Cementitious Materials
SLS	Serviceability Limit State
ss	silica sand
st	stabilizer
ULS	Ultimate Limit State
VMA	Viscosity Modifying Agent
WDP	water Depletion Potential

References

1. Forum, W.E. Net-Zero Industry Tracker 2024 Edition insight report. Technical Report. 2024. Available online: https://reports.weforum.org/docs/WEF_Net_Zero_Industry_Tracker_2024.pdf (accessed on 19 August 2025).
2. Agency, I.E. *Net Zero by 2050—A Roadmap for the Global Energy Sector*; International Energy Agency: Paris, France, 2021.
3. Brucker Juricic, B.; Galić, M.; Marenjak, S. Review of the Construction Labour Demand and Shortages in the EU. *Buildings* **2021**, *11*, 17. https://doi.org/10.3390/buildings11010017.
4. Wangler, T.; Lloret, E.; Reiter, L.; Hack, N.; Gramazio, F.; Kohler, M.; Bernhard, M.; Dillenburger, B.; Buchli, J.; Roussel, N.; et al. Digital Concrete: Opportunities and Challenges. *RILEM Tech. Lett.* **2016**, *1*, 67–75. https://doi.org/10.21809/rilemtechlett.2016.16.
5. Kloft, H.; Gehlen, C.; Dörfler, K.; Hack, N.; Henke, K.; Lowke, D.; Mainka, J.; Raatz, A. TRR 277: Additive manufacturing in construction. *Civ. Eng. Des.* **2021**, *3*, 113–122. https://doi.org/10.1002/cend.202100026.
6. *DIN EN ISO 14025:2011-10*; Umweltkennzeichnungen und -deklarationen_- Typ_III Umweltdeklarationen_- Grundsätze und Verfahren (ISO_14025:2006); Deutsche und Englische Fassung EN_ISO_14025:2011; DIN Media GmbH, Berlin, Germany, 2011. https://doi.org/10.31030/1812964.
7. GCCA. *Cement & Concrete Industry Net Zero Action & Progress Report 2025/26*; Technical Report; Global Cement and Concrete Association (GCCA), London, United Kingdom (UK), 2025.
8. Cherif, C., Ed. *Textile Werkstoffe für den Leichtbau: Techniken - Verfahren - Materialien - Eigenschaften*; Springer: Berlin/Heidelberg, Germany, 2011. https://doi.org/10.1007/978-3-642-17992-1.
9. Backes, J.G.; Traverso, M.; Horvath, A. Environmental assessment of a disruptive innovation: Comparative cradle-to-gate life cycle assessments of carbon-reinforced concrete building component. *Int. J. Life Cycle Assess.* **2023**, *28*, 16–37. https://doi.org/10.1007/s11367-022-02115-z.
10. Glomb, D.; Kustermann, A.; Dauberschmidt, C.; Wolf, B.; Pichlmayr, R. R-Betone mit basaltfaserverstärkter Kunststoffbewehrung: Untersuchungen zum Verbund- und Zugtragverhalten. *Beton-Und Stahlbetonbau* **2024**, *119*, 42–55. https://doi.org/10.1002/best.202300074.
11. Görtz, S.; Lengert, K.; Haack, R. Tragfähigkeit und Anwendungen von Betonbauteilen mit Bewehrung aus basaltfaserverstärktem Kunststoff. *Beton-Und Stahlbetonbau* **2023**, *118*, 607–625. https://doi.org/10.1002/best.202300042.
12. Wolf, B.; Glomb, D.S.; Kustermann, A.; Dauberschmidt, C. Untersuchung des Zug- und Verbundverhaltens von Basaltfaserverstärkter Kunststoff-Stabbewehrung in Beton. *Beton-Und Stahlbetonbau* **2019**, *114*, 454–464. https://doi.org/10.1002/best.201900019.
13. Kloft, H.; Empelmann, M.; Hack, N.; Herrmann, E.; Lowke, D. Bewehrungsstrategien für den Beton-3D-Druck. *Beton-Und Stahlbetonbau* **2020**, *115*, 607–616. https://doi.org/10.1002/best.202000032.
14. Mechtcherine, V.; Michel, A.; Liebscher, M.; Schneider, K.; Großmann, C. Neue Carbonfaserbewehrung für digitalen automatisierten Betonbau. *Beton-Und Stahlbetonbau* **2019**, *114*, 947–955. https://doi.org/10.1002/best.201900058.

15. Görtz, S.; Lengert, K.; Glomb, D.; Kustermann, A.; Dauberschmidt, C.; Burgard, S. Dauerhafte und nachhaltige Brückenkappen aus nichtmetallischer Bewehrung und Recyclingbeton. *Beton-Und Stahlbetonbau* **2025**, *120*, 137–149. https://doi.org/10.1002/best.202400035.
16. Kromoser, B.; Reichenbach, S.; Stoiber, N.; Preinstorfer, P.; Huber, T. *Potentiale von Nichtmetallischer Bewehrung im Infrastruktur-Betonbau NIMETBEW*; Technical Report; Technische Universität Wien, Austria 2022.
17. GmbH, S. Combar Glasfaserverbundbewehrung—Technische Information. 2023. Available online: https://www.schoeck.com/de/gfk-eigenschaften-combar (accessed on 21 April 2026).
18. Leutert, R. Bewehrungen aus Basalt. 2021. Available online: https://www.basalt-fibertec.ch/index.php/produkte/bewehrungen (accessed on 24 March 2026).
19. solidian; kelteks. Solidian REBAR D8-CCE—Technical Product Data Sheet. 2023. Available online: https://www.solidian-kelteks.com/de/produkte/bau/bewehrungen/bewehrungsstaebe/rebar-carbon-detail (accessed on 26 February 2026).
20. Neef, T.; Müller, S.; Mechtcherine, V. 3D-Druck mit Carbonbeton: Technologie und die ersten Untersuchungsergebnisse. *Beton-Und Stahlbetonbau* **2020**, *115*, 943–951. https://doi.org/10.1002/best.202000069.
21. Pavlović, A.; Donchev, T.; Petkova, D.; Staletović, N. Sustainability of alternative reinforcement for concrete structures: Life cycle assessment of basalt FRP bars. *Constr. Build. Mater.* **2022**, *334*, 127424. https://doi.org/10.1016/j.conbuildmat.2022.127424.
22. Sbahieh, S.; Mckay, G.; Al-Ghamdi, S.G. A comparative life cycle assessment of fiber-reinforced polymers as a sustainable reinforcement option in concrete beams. *Front. Built Environ.* **2023**, *9*, 1194121. https://doi.org/10.3389/fbuil.2023.1194121.
23. Dong, S.; Li, C.; Xian, G. Environmental Impacts of Glass- and Carbon-Fiber-Reinforced Polymer Bar-Reinforced Seawater and Sea Sand Concrete Beams Used in Marine Environments: An LCA Case Study. *Polymers* **2021**, *13*, 154. https://doi.org/10.3390/polym13010154.
24. Kumar, D.; Maurya, K.K.; Mandal, S.K.; Mir, B.A.; Nurdiawati, A.; Al-Ghamdi, S.G. Life Cycle Assessment in the Early Design Phase of Buildings: Strategies, Tools, and Future Directions. *Buildings* **2025**, *15*, 1612. https://doi.org/10.3390/buildings15101612.
25. Agustí-Juan, I. Sustainability Assessment and Development of Guidelines for Digital Fabrication in Construction. Ph.D. Thesis, ETH Zurich, Zurich, Switzerland, 2018.
26. Rothe, T.; Gantner, S.; Hack, N.; Hühne, C. Dynamic Winding Process of Individualized Fibre Reinforcement Structures for Additive Manufacturing in Construction. *Open Conf. Proc.* **2023**, *3*. https://doi.org/10.52825/ocp.v3i.187.
27. Thiele, P. Tensile testing and characterisation of BFRP and GFRP reinforcement bars and structural simulation for LCA. **2026**. https://doi.org/10.5281/ZENODO.19973658.
28. Rothe, T.; Pösch, J.; Gantner, S.; Hack, N.; Hühne, C. Optimization of tensile properties and bond behaviour to concrete of fibre reinforcement strands produced within a dynamic fibre winding process. **2023**. https://doi.org/10.5281/ZENODO.8133237.
29. Rothe, T.; Gantner, S.; Hack, N.; Hühne, C. Characterisation of the Alkaline Resistance of Fibre Reinforcement Strands Produced in a Dynamic Fibre Winding Process for {3D} Concrete Printing. In Proceedings of the 2024 fib Symposium (ReConStruct: Resilient Concrete Structures), Christchurch, New Zealand, 11–13 November 2024; pp. 1274–1283.
30. Rennen, P.; Gantner, S.; Rothe, T.; Baz, B.; Nana, S.; Hühne, C.; Hack, N. Structural Evaluation of Shotcrete 3D Printing and Robotic Fiber Winding for Thin Shell Elements. In Proceedings of the IASS 2024 Symposium, Zurich Switzerland, 26–30 August 2024.
31. D30 Committee. *ASTM D7205/D7205M-21*; Test Method for Tensile Properties of Fiber Reinforced Polymer Matrix Composite Bars. ASTM: West Conshohocken, PA, USA, 2026. https://doi.org/10.1520/D7205_D7205M-21.
32. *ISO 14040*; Umweltmanagement - Ökobilanz - Grundsätze und Rahmenbedingungen. DIN Media GmbH, Berlin, Germany, 2021.
33. *ISO 14044*; Umweltmanagement - Ökobilanz - Anforderungen und Anleitungen. Technical Report. DIN Media GmbH, Berlin, Germany, 2021.
34. *EN 15804*; Nachhaltigkeit von Bauwerken – Umweltproduktdeklarationen - Grundregeln für die Produktkategorie Bauprodukte. Technical Report. DIN Media GmbH, Berlin, Germany, 2022.
35. EPD International, 2025. Available online: https://www.environdec.com/library (accessed on 28 January 2026).
36. epd-global. Available online: https://www.epd-global.com/epder/ (accessed on 28 January 2026).
37. EPD Datenbank der Kiwa-Ecobility Experts. Available online: https://www.kiwa.com/de/de/serviceart/zertifizieren/epds/ (accessed on 28 January 2026).
38. Peters, H. Institut Bauen und Umwelt. Available online: https://ibu-epd.com/veroeffentlichte-epds/ (accessed on 5 February 2026).
39. Albrecht, S.V. Life Cycle Inventory for Steel, FRP Reinforcement, and Concrete: Min - Max Values for Different Strength Classes and Manufacturing Methods. **2026**. https://doi.org/10.5281/zenodo.20395834.
40. Hohmann, A. Ökobilanzielle Untersuchung von Herstel- lungsverfahren für CFK-Strukturen zur Iden- tifikation von Optimierungspotentialen. Ph.D. Thesis, Technische Universität München, Germany, 2019.
41. Fořt, J.; Kočí, J.; Černý, R. Environmental Efficiency Aspects of Basalt Fibers Reinforcement in Concrete Mixtures. *Energies* **2021**, *14*, 7736. https://doi.org/10.3390/en14227736.

42. Dressler, I.; Freund, N.; Lowke, D. The Effect of Accelerator Dosage on Fresh Concrete Properties and on Interlayer Strength in Shotcrete 3D Printing. *Materials* **2020**, *13*, 374. https://doi.org/10.3390/ma13020374.
43. Rahul, A.; Mohan, M.K.; De Schutter, G.; Van Tittelboom, K. 3D printable concrete with natural and recycled coarse aggregates: Rheological, mechanical and shrinkage behaviour. *Cem. Concr. Compos.* **2022**, *125*, 104311. https://doi.org/10.1016/j.cemconcomp.2021.104311.
44. Chen, Y.; Chaves Figueiredo, S.; Li, Z.; Chang, Z.; Jansen, K.; Çopuroğlu, O.; Schlangen, E. Improving printability of limestone-calcined clay-based cementitious materials by using viscosity-modifying admixture. *Cem. Concr. Res.* **2020**, *132*, 106040. https://doi.org/10.1016/j.cemconres.2020.106040.
45. Obermeier, N.; Richter, C.; Wiese, F.; Stengel, T. Low Global Warming Potential and Resource-Efficient 3D Printing Cement-Based Concrete. In *4th fib International Conference on Concrete Sustainability (ICCS2024)*; Barros, J.A.O., Cunha, V.M.C.F., Sousa, H.S., Matos, J.C., Sena-Cruz, J.M., Eds.; Series Title: Lecture Notes in Civil Engineering; Springer Nature: Cham, Switzerland, 2024; Volume 574, pp. 422–429. https://doi.org/10.1007/978-3-031-80724-4_52.
46. Senf, F.; Javed, R.; Funke, H.; Gelbrich, S. Enhanced environmental sustainability of 3D-printed concrete mixtures based on calcium sulfoaluminate (CSA) and blast furnace cement (CEM III/B). *MATEC Web Conf.* **2025**, *409*, 06004. https://doi.org/10.1051/matecconf/202540906004.
47. Kalthoff, M.; Raupach, M.; Matschei, T. Investigation into the Integration of Impregnated Glass and Carbon Textiles in a Laboratory Mortar Extruder (LabMorTex). *Materials* **2021**, *14*, 7406. https://doi.org/10.3390/ma14237406.
48. Stengel, T.; Kustermann, A. LCA of Recycled and Normal Aggregate Concrete—Circular Versus Linear Economy. In *4th fib International Conference on Concrete Sustainability (ICCS2024)*; Barros, J.A.O., Cunha, V.M.C.F., Sousa, H.S., Matos, J.C., Sena-Cruz, J.M., Eds.; Series Title: Lecture Notes in Civil Engineering; Springer Nature: Cham, Switzerland, 2024; Volume 574, pp. 341–351. https://doi.org/10.1007/978-3-031-80724-4_42.
49. European Automobile Manufacturers' Association. NOx emissions from the EU heavy truck fleet by Euro classes. Available online: https://www.acea.auto/figure/nox-emissions-from-the-eu-heavy-truck-fleet-by-euro-classes/ (accessed on 5 May 2026).
50. Dorer, C.; Hahn, J. Energetische Optimierung der Betonherstellung im Transportbetonwerk - Bestandsaufnahme und Ableitung von Optimierungspotenzialen. Final Report, Institut für Werkstoffe im Bauwesen (IWB), Universität Stuttgart, 2015. Commissioned by Forschungsgemeinschaft Transportbeton e.V. (FTB), Berlin, Germany. In German
51. Scrivener, K.L.; John, V.M.; Gartner, E.M. Eco-efficient cements: Potential economically viable solutions for a low-CO2 cement-based materials industry. *Cem. Concr. Res.* **2018**, *114*, 2–26. https://doi.org/10.1016/j.cemconres.2018.03.015.
52. *Circularity Gap Report 2023*; Technical Report; Circle Economy: Amsterdam, The Netherlands, 2023.
53. International Federation for Structural Concrete.; International Federation for Structural Concrete. FRP reinforcement in RC structures. In *Number 40 in Bulletin / International Federation for Structural Concrete Technical Report*; International Federation for Structural Concrete (fib): Lausanne, Switzerland, 2007.
54. Micelli, F.; Nanni, A. Durability of FRP rods for concrete structures. *Constr. Build. Mater.* **2004**, *18*, 491–503. https://doi.org/10.1016/j.conbuildmat.2004.04.012.
55. D'Antino, T.; Pisani, M.A. Long-term behavior of GFRP reinforcing bars. *Compos. Struct.* **2019**, *227*, 111283. https://doi.org/10.1016/j.compstruct.2019.111283.
56. D'Antino, T.; Pisani, M.A.; Poggi, C. Effect of the environment on the performance of GFRP reinforcing bars. *Compos. Part B Eng.* **2018**, *141*, 123–136. https://doi.org/10.1016/j.compositesb.2017.12.037.
57. Spelter, A.; Bergmann, S.; Bielak, J.; Hegger, J. Long-Term Durability of Carbon-Reinforced Concrete: An Overview and Experimental Investigations. *Appl. Sci.* **2019**, *9*, 1651. https://doi.org/10.3390/app9081651.
58. Deutscher Ausschuss für Stahlbeton (DAfStb), DAfStb-Richtlinie: Betonbauteile, nichtmetallische Bewehrung, Edition 2024-01, DIN Media GmbH: Berlin, Germany 2024. In German.
59. *DIN 488-1:2009-08*; Betonstahl_- Teil_1: Stahlsorten, Eigenschaften, Kennzeichnung. DIN Media GmbH, Berlin, Germany https://doi.org/10.31030/1520610.
60. Steckbauer, M.A.; Evangelatos, A.; Galler, R. Softwaregestütze Bemessung von Betonbewehrung aus Basaltfasern. *BHM Berg.-Und Hüttenmännische Monatshefte* **2024**, *169*, 643–648. https://doi.org/10.1007/s00501-024-01528-7.
61. Stoiber, N.; Hammerl, M.; Kromoser, B. Cradle-to-gate life cycle assessment of CFRP reinforcement for concrete structures: Calculation basis and exemplary application. *J. Clean. Prod.* **2021**, *280*, 124300. https://doi.org/10.1016/j.jclepro.2020.124300.
62. Sergis, V.; Ouellet-Plamondon, C.M. Automating mix design for 3D concrete printing using optimization methods. *Digit. Discov.* **2022**, *1*, 645–657. https://doi.org/10.1039/D2DD00040G.
63. Hill, C.; Norton, A. LCA Database of Environmental Impacts to Inform Material Selection Process; DACOMAT: Paris, France, 2018, 1-32 2020.

64. Laiblová, L.; Pešta, J.; Kumar, A.; Hájek, P.; Fiala, C.; Vlach, T.; Kočí, V. Environmental Impact of Textile Reinforced Concrete Facades Compared to Conventional Solutions—LCA Case Study. *Materials* **2019**, *12*, 3194. https://doi.org/10.3390/ma12193194.
65. Backes, J.G.; Del Rosario, P.; Luthin, A.; Traverso, M. Comparative Life Cycle Assessment of End-of-Life Scenarios of Carbon-Reinforced Concrete: A Case Study. *Appl. Sci.* **2022**, *12*, 9255. https://doi.org/10.3390/app12189255.

Disclaimer/Publisher's Note: The statements, opinions and data contained in all publications are solely those of the individual author(s) and contributor(s) and not of MDPI and/or the editor(s). MDPI and/or the editor(s) disclaim responsibility for any injury to people or property resulting from any ideas, methods, instructions or products referred to in the content.